Samuli Suvisto

Effects of Dexmedetomidine on the cortical activity of neonates

School of Electrical Engineering

Thesis submitted for examination for the degree of Master of Science in Technology.

Espoo October 20, 2018

Thesis supervisor:

Prof. Ilkka Laakso

Thesis advisors:

PhD. Anton Tokariev

Prof. Sampsa Vanhatalo

Aalto University
School of Electrical
Engineering

AALTO UNIVERSITY
SCHOOL OF ELECTRICAL ENGINEERING

ABSTRACT OF THE
MASTER'S THESIS

Author: Samuli Suvisto

Title: Effects of Dexmedetomidine on the cortical activity of neonates

Date: October 20, 2018 Language: English Number of pages: 7+58

Department of Electrical Engineering and Automation

Professorship: Electromagnetics in Health Technologies

Supervisor: Prof. Ilkka Laakso

Advisors: PhD. Anton Tokariev, Prof. Sampsa Vanhatalo

This thesis aimed to study the effects of dexmedetomidine on the cortical activity of neonates by statistically analyzing electroencephalographic (EEG) recordings. Dexmedetomidine is a sedative that has been proven to be effective and safe to use with adults, however, its neurocognitive effects on newborns remain unclear. The used dataset consisted of 21 neonates that had been treated with dexmedetomidine. For quantifying the recordings, a set of eight computational features were selected that represented correlation of phase, synchrony, spectral properties as well as multifractality of the signals. In this thesis, dexmedetomidine was found to affect different measures of synchrony and phase correlation. Furthermore, it was shown that hour-long recordings do not seem to be needed for examining the neurocognitive effects of dexmedetomidine as all of the effects could be seen within the following ten minutes after the subjects had received the drug.

Keywords: EEG, Neonate, Dexmedetomidine, Drug, Sedative

AALTO-YLIOPISTO
SÄHKÖTEKNIIKAN KORKEAKOULU

DIPLOMITYÖN
TIIVISTELMÄ

Tekijä: Samuli Suvisto

Työn nimi: Dexmedetomidiinin vaikutus vastasyntyneiden kortikaaliseen aktiivisuuteen

Päivämäärä: October 20, 2018 Kieli: Englanti Sivumäärä: 7+58

Sähkötekniikan ja automaation laitos

Professuuri: Sähkömagnetiikka terveysteknologioissa

Valvoja: Prof. Ilkka Laakso

Ohjaajat: FT Anton Tokariev, Prof. Sampsa Vanhatalo

Tämän työn tarkoituksena oli tutkia dexmedetomidiinin vaikutusta vastasyntyneiden kortikaaliseen aktiivisuuteen analysoimalla tallennettuja aivosähkökäyriä (EEG) tilastollisesti. Dexmedetomidiini on sedatiivi, joka on osoitettu tehokkaaksi ja turvalliseksi aikuisilla. Sen aiheuttamia neurokognitiivisia vaikutuksia vastasyntyneillä ei kuitenkaan tunneta. Tutkimuksen aineisto koostui 21:stä vastasyntyneestä, jotka kaikki olivat saaneet dexmedetomidiinia. Työssä valittiin kahdeksan erilaista muuttujajoukkoa kuvaamaan tallenteita. Nämä muuttujajoukot kuvasivat signaalien vaiheiden välistä korrelaatiota, synkroniaa, taajuusjakaumaa ja multifraktaalisuutta. Dexmedetomidiinin havaittiin vaikuttavan signaalien vaiheiden väliseen korrelaatioon sekä synkroniaan. Tämän lisäksi tässä työssä osoitettiin, että tuntien pituiset aivosähkökäyrätallenteet eivät ole tarpeellisia dexmedetomidiinin neurokognitiivisten vaikutusten tutkimiseen, sillä kaikki vaikutukset havaittiin lääkkeen antamista seuranneen kymmenen minuutin aikana.

Avainsanat: EEG, Vastasyntynyt, Dexmedetomidiini, Lääkeaine, Sedatiivi

Preface

I would like to take this opportunity to thank the research team at the Baby Brain Activity (BABA) clinical research center at the Helsinki Children's Hospital for their support while I was working on my thesis. I'm especially grateful to my advisors Prof. Sampsa Vanhatalo and PhD. Anton Tokariev for their immense guidance during this process. I would also like to thank Prof. Ilkka Laakso for supervising this work.

Otaniemi, 18.9.2018

Samuli Suvisto

Contents

Symbols and abbreviations

Symbols

τ	Time lag
j	Imaginary unit
$P_\tau(a, b)$	Joint probability
$\theta(a, b)$	Phase difference
E	Expected value
W	Sum of ranked values
R	Sum of ranks
$F_q(s)$	Fluctuation function
$Y(i)$	Signal profile
$D(q)$	q-order singularity dimension
$H(q)$	q-order Hurst exponent
$h(q)$	q-order singularity exponent
σ	Standard deviation
r_s	Spearman's rho
Δ	Delta values

Abbreviations

aEEG	Amplitude-integrated Electroencephalography
ASI	Activation Synchrony Index
BL	Baseline epoch
CA	Conceptional Age
cPSD	Cross Power Spectral Density
DFA	Detrending Fluctuation Analysis
DX	Dexmedetomidine epoch
ECG	Electrocardiogram
EDTF	Energy-Weighted Temporal Dependency Function
EEG	Electroencephalography
EOG	Electrooculography
FFT	Fast Fourier Transform
HIE	Hypoxic-Ischemic Encephalopathy
IQR	Interquartile Range
LI	Lower 5th Index
MFDFA	Multifractal Detrended Fluctuation Analysis
NICU	Neonatal Intensive Care Unit
NC	Nestedness Coefficient
PLI	Phase Lag Index
PLV	Phase Locking Value
PSD	Power Spectral Density
rEEG	Range-Electroencephalography
SAT	Spontaneous Activity Transient
wPLI	Weighted Phase Lag Index

1 Introduction

Neonatal intensive care unit is a place for infants suffering from various different complications or disorders and in need of medical care. In intensive care, the infants are often treated with drugs, frequently to provide sedation or analgesia. Dexmedetomidine has been previously used as a sedative with neonates. It is an agonist for $\alpha 2$-adrenoreceptors in the central nervous system. Dexmedetomine's advantages on adults include minimal lowered respiration rate, sleep like induced sedation and has short half-life of roughly from 1.5 to 3 hours, meaning that it is cleared from the blood stream relatively fast. [1, 2, 3]

However, even though previously being used with infants and proven to be effective and safe with adults, the use of dexmedetomidine in Finland diminished after concerns on the safety of dexmedetomidine on neonates were raised [4]. Although it is possible that these concerns could be related to cardiovascular effects, such as bradycardia, and not neurocognitive complications. [1, 2, 5] Studies of dexmedetomidine decreasing the blood flow in the brain on adults have been published and thus, the effects of dexmedetomidine could also be seen in the cortical activity as well [6].

The goal of this thesis is to study if the administration of dexmedetomidine to babies would affect their brain activity. The dataset used in this thesis consisted of electroencephalographic recordings of 22 neonates, both preterm and fullterm. However, only recordings from 21 subjects were analyzed as one subject was rejected due to having a recording only after receiving the drug. Most subjects had recordings taken both before and after the subjects received the drug and most of them had a duration of roughly four hours (8 hours in total per baby). By examining the effects, it is also hoped to shed light on whether the dexmedetomidine would be safe to use in neonates. The recordings contained four channels and the studied frequency bands ranged from 0.2 to 35 Hz. A total of eight different computational features were selected to quantify the data and to be statistically analyzed. These features were selected based on Julia Jaatela's previous work and other literature as well as on advice from a medical doctor [7]. This thesis consists of two different studies for determining:

1. What are the hour-long effects of dexmedetomidine?

2. What are the short-term effects seen immediately after the dosing?

Julia Jaatela's thesis, titled "Computational features of neonatal EEG monitoring after asphyxia", was used as a baseline and roughly followed for the applicable parts when carrying out the studies for this thesis.

For determining the hour-long effects of dexmedetomidine, as much as possible of all the recordings were used to plot time-trends of the eight different computational features. The time-trends consisted of all of the subjects plotted in the same figure together with a mean value. These time trends were then visually analyzed to determine any changes in the cortical activity.

The second study for determining the short-term effects consisted of two different statistical analyses. For this study a 12-minute baseline epoch just before the drug administration and a 10-minute epoch after the drug were extracted. The first statistical analysis then had the feature values of these epochs compared to determine if there were any differences between them. For the second statistical analysis we subtracted the baseline value from the postdrug value and studied whether the change correlated with the baseline value. The second analysis was included as we suspected that the background state of the subject might affect the postdrug feature values.

Finally, other clinical factors besides dexmedetomidine affecting the selected features were examined. The clinical factors were administration of fentanyl, conceptional age and background diagnosis. These factors were compared against the baseline values of the features and analyzed for correlations.

2 Background

The aim of this section is to introduce the background of the study field regarding this thesis. In this section we first take a look on EEG on a basic level. After this, the differences between neonatal EEG and the EEG of an adult are discussed. Together with the neonatal EEG, the neonatal intensive care unit (NICU) is introduced as it is the environment where the subjects were treated and the EEG recordings carried out. For the subjects to be critically ill and treated at NICU is an essential part of the study. Finally, EEG analysis and monitoring is discussed.

2.1 Electroencephalography

The brain of an adult consists of up to a 10^{11} neurons and even a greater amount of other type of cells, such as various glial cells, that make up a major part of the volume of the brain [8]. The neurons process information and communicate with electrical signals that are passed through junctions, called synapses, that connect two separate neurons. EEG is a method for studying this electrical activity of the cerebral cortex, that is the outer layer of brain. However, as the potentials of a single neuron or synapse are too weak to be detected by EEG, the detected brain waves consist of potentials that are a sum of a larger population of postsynaptic action potentials [9].

The electrical activity recorded in EEG is the potential difference between two distinct areas on the scalp. This potential difference can be either between two electrodes or every electrode in respective to an common reference. The recorded activity is conventionally divided into four different frequency bands, delta (0.5–4 Hz), theta (4–8 Hz), alpha (8–13 Hz) and beta (13–30 Hz) [10]. In adults, delta waves are present during deep sleep. However, they are also normal in awake neonates. Theta waves are typically found during emotional stress but are also common in many disorders of the brain. Alpha waves are normally found in EEGs of adults who are awake and resting, while beta waves are occur when the nervous system is activated. [8]

Traditionally EEG is noninvasive and voltage sensitive electrodes are placed on top of the scalp. The number of electrodes used for recording the brain activity can vary depending on the situation, however, their placement usually follows an international 10–20 system [11]. The placement of electrodes is determined with the help of anatomic landmarks found in the skull to accommodate for the differences in head sizes and shapes [12]. In this system, every electrode position is designated with a name that comprises of a letter and a number. The letters determine the region that the electrode is located in, F for frontal, T for temporal, P for parietal and O for occipital lobes. In addition, a letter C is also used and stands for central. The numbers are assigned based on the hemisphere, even for right and odd for left hemisphere. Thus, every electrode position has a unique identifier. The electrode placement is illustrated in Figure 1. For practical reasons, such as the small head size, the EEG of neonates is often recorded with only a few electrodes per hemisphere following the international 10–20 system.

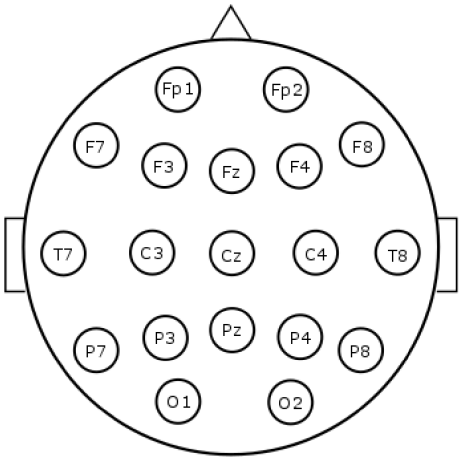

Figure 1: An illustration of the international 10–20 system showing the placement of the electrodes.

The advantages of EEG include high temporal resolution, meaning that it can be used for high precision time measurements. This attribute is essential, as the electrical activity of the brain fluctuates rapidly. The EEG devices today can detect these fluctuations with resolutions down to less than a millisecond [13]. On the other hand, while having a high temporal resolution, the disadvantages of EEG include poor spatial resolution. Even though this is a direct result of the limited number of electrodes used in EEG, another cause is volume conduction. Volume conduction is an effect that results from measuring the electrical activity from the scalp when the source of the potentials is located at distance inside the brain. Thus, the same source can affect multiple electrodes. [14]

Another major challenge in EEG recordings is the presence of artifacts. These are activities that can be observed in EEG but are not of cerebral origin. Artifacts are common in all electrical recordings. Common causes for artifacts found in EEG recordings are movements of the electrodes and the electrical activity of locations other than the brain [15]. Typical electrical activities of muscles observed in the EEG are body movements such as eye movements, swallowing, blinking and respitory movements [16]. In addition, the QRS complex of electrocardiogram (ECG) can frequently result in an artifact to be seen in EEG [17]. Besides artifacts of physiological origin artifacts can arise from sources that are external of the body. An example of such artifact is the capacitive coupling of alternating current from power lines or equipment in the environment. This results in an artifact present at 60 Hz. [18] Artifacts in EEG are often identifiable as sudden and great rises in the amplitude of the recording. In identifying the artifacts, other electrical recordings are often used, such as ECG or electrooculography (EOG) [17]. Other methods for dealing with recordings corrupted by artifacts include manually removing parts of recordings as well as filtering. Filtering the artifacts can be especially practical, if the artifacts are located in specific frequencies. Also artifacts that reside in frequencies outside the band of interest, meaning that the frequencies are either high or low enough, can be effectively filtered.

2.2 Neonatal EEG and intensive care unit

The development of the nervous systems starts already in the early weeks of gestation with the differentiation of nervous cells and can be considered to continue throughout the lifespan [19]. During the early development of the brain, cortical activity and sensory inputs play critical roles resulting in modifications of the brain. These modifications take place via branching of axons, controlled cell death as well as through the addition, removal and stabilization of synapses [20]

Due to the development of the brain, the neonatal cortical activity that can be recorded with EEG possesses unique features. Most importantly, the background state of EEG recorded from a neonatal brain differs significantly from adult one. One of the common distinguishing aspects of preterm EEG, babies born before age of 37 weeks, is the discontinuity compared to the EEG of an adult. Thus the preterm EEG is normally categorized into either being continuous or discontinuous. With preterm infants intermittent burst of activity are common in presence of otherwise discontinuous EEG [21]. These bursts of activity are called spontaneous activity transients (SATs) [22]. These are thought to originate from the subplate zone of neonatal brain, which is located underneath the cortical layer. The cortical subplate zone is also considered to regulate the cortical activity of preterm infants over cortical connections [23]. As the infant matures, the EEG becomes more and more continuous and the SATs disappear together with the subplate as the infant reaches term age [24]. The activity of a full-term infant is continuous during both, wakefulness and active sleep [21]. SATs are considered to correspond to the brain wiring itself [24].

Another difference between the cortical activity of preterm infants and adults is the expression of sleep stages. As described earlier the EEG of preterms with conceptional age (CA) below 32 weeks is discontinuous and the waking and sleeping states cannot be distinguished from each other. After an age of 32 weeks CA, a differentiation between active sleep, quiet sleep and wakefulness begins. However, it is only after 36 weeks CA when these states can be correlated with three different EEG patterns. [21] The quiet sleep is characterized with discontinuity while active sleep is continuous. [25]

NICU is a place for treating and monitoring critically ill neonates in need of special treatment. Reasons behind the neonate requiring intensive care include premature birth, difficulties in breathing, infections or birth defects, neurological disorders, labor complications or problems caused by the mother's disease. [26]

As the neonates are critically ill, they are often treated with drugs, such as sedatives. The drug of interest in this thesis, dexmedetomidine, is one example of these sedatives. One common reason for a neonate to be administered dexmedetomidine has been hypoxic-ischemic encephalopathy (HIE), which is brain damage caused by asphyxia, the lack of oxygen in the brain. The standard treatment for moderate or severe HIE is lowering the body treatment of the neonate down to 33-34°C for 72 hours, after which the body temperature is raised slowly back to normal [27]. Preceding the hypothermia treatment, the neonates often need to be sedated to lessen the stress and the tremor of the baby. Although the cardiovascular effects of

dexmedetomidine in neonates are known, the neurocognitive effects have not been studied extensively and remain unclear [28, 29]. Generally, concerns of anesthetics being linked to inducing apoptosis in the developing brain have been raised in recent years, especially during general anesthesia [30, 31, 32].

It has been stated that conditions associated with prematurity and also treatment during the infants stay at NICU may account for the subsequent neurocognitive conditions or outcomes [22]. This could be due to the timing of when the preterm babies are admitted to NICU often roughly corresponding to the third trimester of the pregnancy, which is the period when the growth of long-range connections in brain occurs.

2.3 EEG analysis and monitoring

EEG is a powerful tool for both studying and monitoring the brain activity of neonates. Common fields of interest in EEG studies include the study of drug effects, where EEG is statistically analyzed for tracing drug-induced and time-related changes in the frequency and amplitude of EEG signals. In studies of this kind, EEG is recorded both before and after the drug dosing. This way the EEG after the dosage can be statistically compared to the baseline EEG (before the dosage). Commonly EEG is used to study the drug effects both spatially as well as temporally. Despite the poor spatial resolution, EEG can be used to, at minimum, determine if the drug-induced changes are restricted to either hemisphere of the brain. [33]

In computational EEG analysis the data is often described with specific computational features. In essence, these features are quantitative parameters used for extracting information that might not be possible to see or quantify visually. Some computational features for analyzing neonatal brain activity have been adopted from the ones used for adults, however, metrics have also been developed and tailored for neonatal EEG directly. In EEG analysis, the focus is usually in the main components of EEG: amplitude, frequency and phase [34]. Often in EEG analysis the discrete values used for representing the data are found to have interdependencies such as covariances or correlations. Thus for instance, analyzing the degree of synchrony between two signals that originate from different spatial location of the brain is common.

EEG monitoring, especially amplitude-integrated EEG (aEEG), is often used for observing the cerebral activity of neonates in intensive care. As the background activity of EEG can be used to predict the outcome of both term asphyxiated infants and preterm infants. In addition, aEEG is a powerful tool in detecting seizures and can also be used to monitor responses to drug therapy and depth of anesthesia [35, 36, 33]. EEG has been shown to be sensitive towards being modulated by various drugs. Examples of drug effects on EEG activity include: increase of power in specific frequency bands, depression of background activity and obscuring sleep-wake cycles.[22, 33, 37] However, aEEG should be used as a complement to normal EEG when possible, and due to its unique nature, successful EEG monitoring requires collaboration between neonatologists and clinical neurophysiologists [36].

3 Materials and methods

In this section the different methods used to assess the effect of dexmedetomidine are introduced. First the dataset and different pre-processing steps taken are presented following with the different computational features. From the computational features the decisions to include them together with the actual computation steps are discussed. In addition, different statistical methods for evaluating the computational features are presented. Finally, as the effects of dexmedetomidine were assessed on multiple different time scales, the different studies performed are introduced. All of the signal processing was carried out and the features computed in MATLAB.

3.1 Dataset

The dataset for this thesis consisted of four channel EEG recordings of 22 neonates, both full term and preterm. These recordings were collected over a time-period from April 2013 to September 2016. Out of the 22 subjects, 21 had recordings both before and after receiving the drug. One subject had a recording only after the drug and was thus rejected. Most of the recordings had a length of 4 hours, although a few subjects had recordings as short as 1 hour. The four channels recorded were two frontal channels, F3 and F4, and two parietal channels, P3 and P4. The reference point shared by all of the four channels was nasion, a point between the eyes. The location of these electrodes on the scalp can be seen in Figure 2. The recordings of all of the subjects had a sampling frequency of 250 Hz, with an exception of two subjects having a sampling frequency of 500 Hz. The conceptional age of the subjects ranged from 197 to 306 days, as it was reported, and had an average of 38.68 ± 3.61 (mean $\pm$ SD) weeks. As the subjects had numerous different diagnoses and were not homogeneous, they were categorized in to four different categories based on the severity. These categories and the distribution of subjects in to them is explained in more detail in Section 3.5.3.

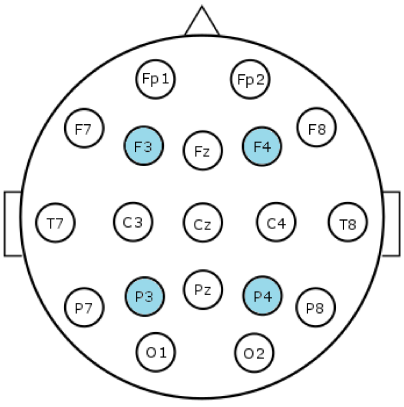

Figure 2: An illustration of the 10-20 system where positions of the channels used in this thesis are highlighted in blue.

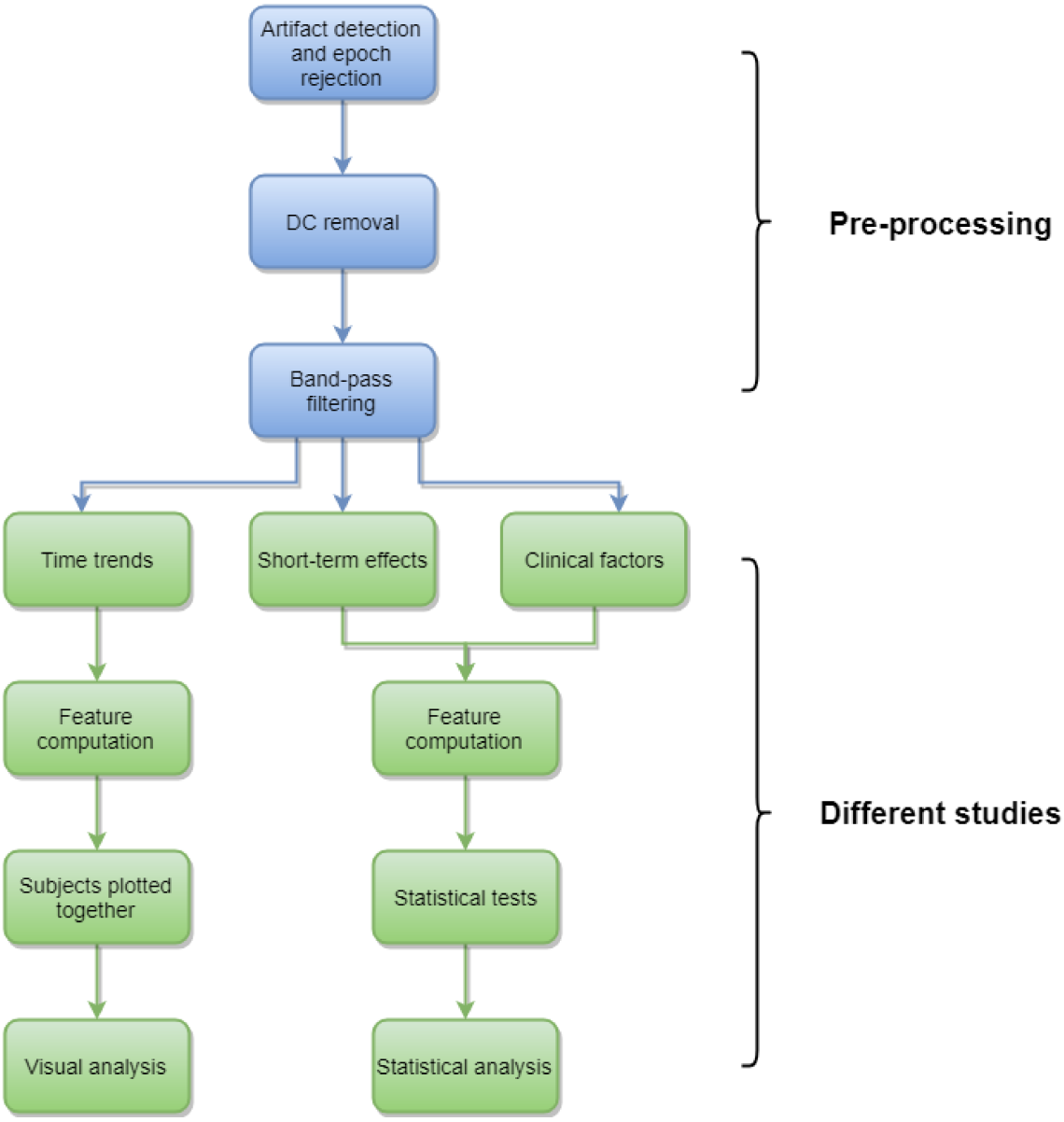

Figure 3: A flow chart presenting the different steps of data processing and analyzing taken in this thesis.

3.2 Data pre-processing

After visual analysis, most recordings were found to contain artifacts that had to be removed before other pre-processing could take place. However, this was to be expected as clinical data was used and it almost always contains artifacts. If the artifacts were not removed, they could affect the data in undesired ways and reduce the quality of the data. For example, high amplitude peaks caused by artifacts could lead to ringing when the signals are filtered. Thus, an artifact detection system was developed for detecting different types of artifacts. The principle of this system was that it most importantly removed all high amplitude artifacts, as well as marked the signal for lower amplitude artifacts that could alter the results of the research later on.

After the high amplitude artifacts were removed, the DC component was then removed from the signals by computing the mean from the whole length of the recording and then subtracting the mean value from the signal. The signals were then band-pass filtered. The band-pass filtering was carried out with separate fifth order Butterworth high-pass and a seventh order Butterworth low-pass filters with cutoff frequencies of 0.2 Hz and 35 Hz, respectively. The signals were filtered in both forward and reverse directions to avoid phase shifting. Finally, the the recordings of the two subjects with sampling frequency of 500 Hz were down sampled to 250 Hz.

3.2.1 Artifact detection

The artifact detection algorithm consisted of three separate detectors, amplitude-based as well as a high frequency and low frequency artifact detectors. The amplitude-based detector had a threshold of 500 μV for the maximum of EEG, above which the signal was assumed to contain an artifact. Moreover, when a peak exceeding 500 μV was found, the threshold was lowered to 300 μV for 7 seconds around the artifact. This was done to detect the "secondary" artifacts and ringing caused by the large artifact.

For both the low and high frequency artifact detectors, the signals were cut down in to 2.5 min epochs, after which Welch's power spectral density was calculated for all of the epochs. The frequency bands for the low and high frequency artifacts were chosen to be 0.15–0.5 Hz and 15–25 Hz, respectively. The powers transferred over these bands were then normalized by dividing them with the power transferred over a frequency band from 1 Hz to 10 Hz and plotted in histograms. This was done to visualize the distribution of the power transferred in these epochs and the frequency bands in question. As the power spectral density distributions were found to follow normal distribution, outlier epochs were assumed to contain artifacts. For the assumption, 95 percentile was chosen to be the threshold and epochs with higher values were considered as outliers. These assumptions were verified after visually analyzing the validity of the artifact detectors. The normalized high frequency power spectral densities of each epoch can be found in Figure 4.

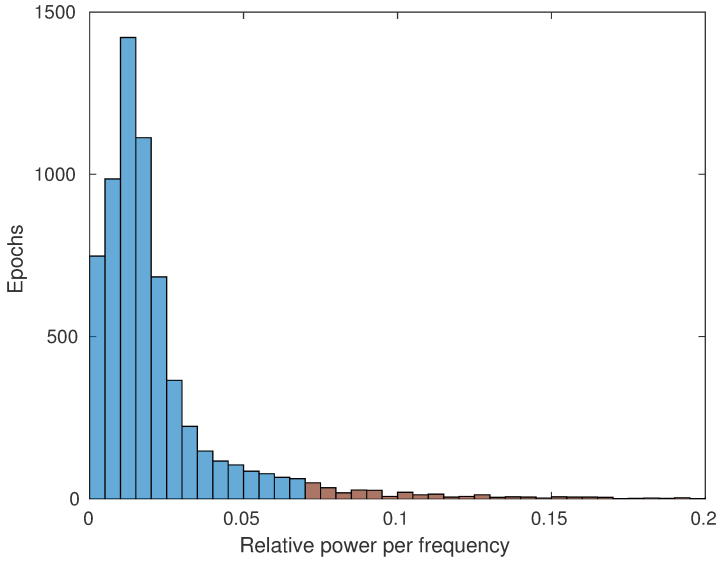

Figure 4: A histogram showing the distribution of the power transferred over a frequency band of 15–25 Hz in relation to the power over 1–10 Hz in different epochs. The 95th percentile is shown in blue and all of the brown epochs are assumed to contain artifacts.

Three different artifact masks containing the temporal location of artifacts were then created with the described artifact detectors. While both the low frequency and the high frequency artifact masks marked the whole 2.5 min epoch if it contained artifacts, the amplitude mask had a resolution up to a single datapoint. Figure 5 shows the working principle of the artifact detectors.

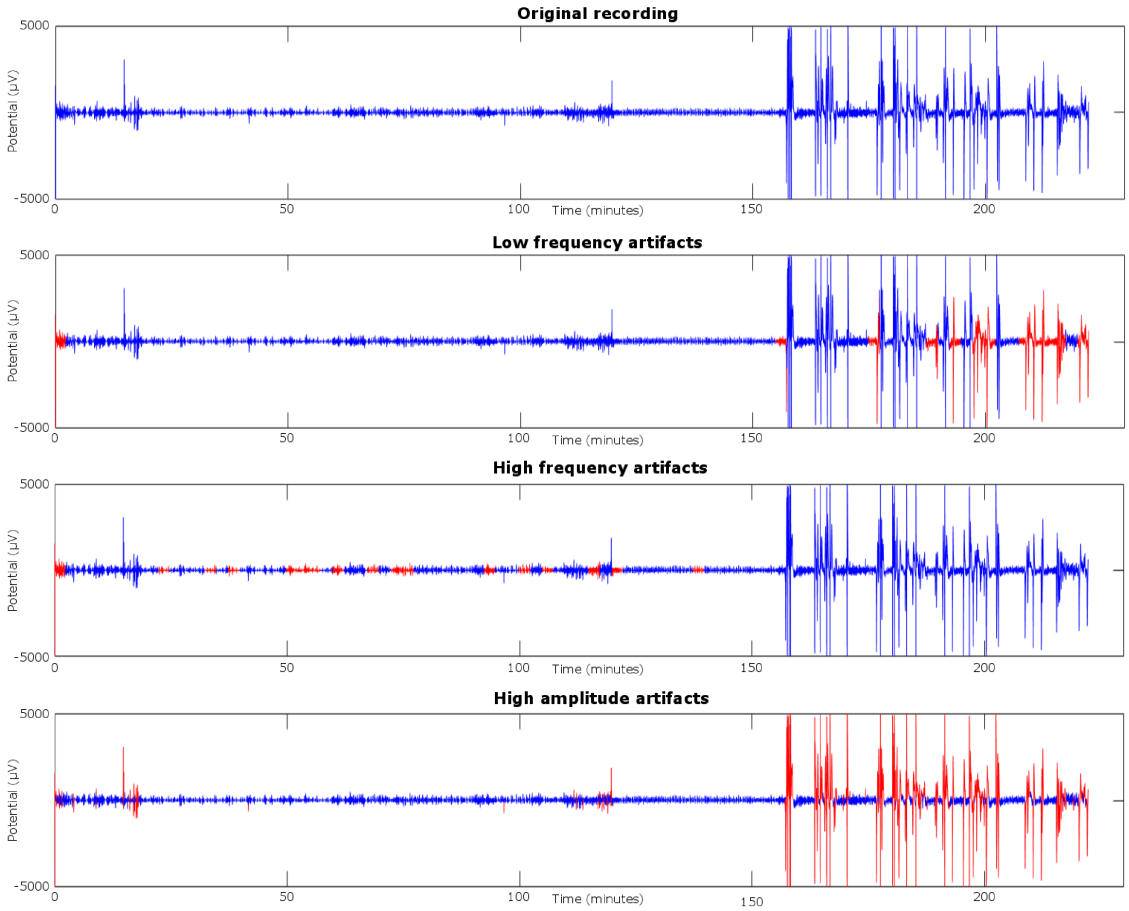

Figure 5: The working principle of the three artifact detectors. The original signal is plotted in blue, while the artifact containing data is highlighted in red.

3.3 Computational features

For analyzing and providing a comprehensive assessment on the effects of dexmedetomidine to cortical activity, a set of eight different computational features were selected. These features can roughly be categorized to features measuring different kinds of synchronizations and to non-synchronization metrics. Different measures of synchrony and correlation chosen for the studies were activation synchrony index (ASI), weighted phase lag index (wPLI) and nestedness coefficient (NC). The rest of the features included measures for peak-to-peak amplitude, spectral density and more. The computational features presented in this section had different montages and or frequency bands that are listed, together with a complete list of the used features, in Table 1. These frequency bands followed roughly the alpha, beta, delta and theta frequency ranges. All of the bipolar montages were computed from the four monopolar channels F3, F4, P3 and P4.

Table 1: Summary of the computational features used in all of the studies conducted. Table presents the feature names, types, montages and frequency bands. The last column presents the number of different variables obtained for each feature.

Feature	Type	Montages	Frequency bands (Hz)	Number of variables
ASI	Interhemispheric synchrony	F3P3—F4P4 F3—P3 F4—P4 F3—F4 P3—P4	1.5—20	5
wPLI	Phase-phase synchrony	F3—P3 F4—P4 F3—F4 P3—P4	0.25—3, 3—8, 8—15 and 15—30	16
NC	Phase-amplitude synchrony	F3 F4 P3 P4	3—8, 8—15 and 15—30	12
PSD	Spectral density	F3P3 F4P4 F3F4 P3P4 F3 F4 P3 P4	1—3, 3—8, 8—15 and 15—30	32
cPSD	Spectral density	F3P3—F4P4 F3—P3 F4—P4 F3—F4 P3—P4	1—3, 3—8, 8—15 and 15—30	20
aEEG	Peak-to-peak amplitude	F3P3 F4P4 F3F4 P3P4 F3 F4 P3 P4	2—15	16
rEEG	Peak-to-peak amplitude	F3P3 F4P4 F3F4 P3P4 F3 F4 P3 P4	0.5—35	24
MFDFA	Multifractality	F3P3 F4P4 F3F4 P3P4 F3 F4 P3 P4	0.2—35	32

3.3.1 Activation synchrony index

Activation synchrony index (ASI) quantifies the co-occurrence of SATs between two EEG signals. It was developed by Räsänen et al. [38] as an objective measure to quantify the interhemispheric synchrony. Interhemispheric synchrony is one of the key features when analyzing the background activity of neonatal EEG. This interaction of the hemispheres has been shown to increase with age of the neonate, and on the other hand, decrease with different disorders in the brain. ASI is based on computing statistically the time delay between quantized amplitude envelopes of two EEG signals [38].

Following the work of Räsänen et al. [38] the signals were first pre-processed. The pre-processing consisted several steps, first of which was the down-sampling the signals to 50 Hz from 250 Hz. In addition, a finite impulse response high-pass filter of first order was used to emphasize higher frequencies that are related to SATs. After filtering, the amplitude envelopes of the two signals were then computed with the use of fast Fourier transformation (FTT). The FTT used a sliding Hamming window with a 100 ms step size. The width of the Hamming window was 2 seconds. After FFT the amplitudes of frequency bins corresponding to a range from 1.5 Hz to 20 Hz were summed up.

Next step in the pre-processing of ASI was the quantization the envelopes into Q discrete levels. A random subset of samples was clustered with standard k-means algorithm, after which every sample was assigned to the closest resulting cluster. This resulted in two sequences that are discrete and correspond to the two input signals A and B. The purpose of quantization of the envelopes is to be able to represent the two signals with a small enough number of levels that allow reliable estimation of joint probabilities of amplitude value combinations between these two signals. This is due to the joint probability space increasing exponentially with the number of quantization levels [38]. The chosen number of quantization levels in this study was 8, based on the previous work of both Räsänen et al. [38] and Koolen et al. [39].

After pre-processing, the next step was to measure the dependency of the computed signal states. The dependency was measured by calculating an energy-weighted temporal dependency function (EDTF) between the quantized envelopes. EDTF measures the statistical dependencies of all signal state pairs with different temporal delays. In order to measure the dependency of signal energy, as opposed to states, every state pair is weighted with the product of the amplitude values of the associated states. EDTF can be expressed as the following equation:

$$\mathrm{EDTF}(\tau) = \sum_{a,b} E(a)E(b)\frac{P_\tau(a,b)^2}{P(a)P(b)}, \tag{1}$$

where $P_\tau(a,b)$ is the joint probability for observing levels a and b in signals A and B respectively, when signal B is delayed by τ. $P(a)$ and $P(b)$ are the individual probabilities for observing these levels. The time delay of τ had a range from -5 to $+5$ seconds. $E(a)$ and $E(b)$ denote the amplitudes corresponding to quantization levels a and b.

For measuring the relative EDTF values at different lags, EDTFs global minimum was subtracted from all EDTF values. The final ASI value was then calculated as a ratio of the EDTF value at $\tau = 0$ divided by the mean EDTF over the entire range of -5 to $+5$ s:

$$\mathrm{ASI} = \mathrm{EDTF}_{\mathrm{norm}}(\tau = 0) \Big/ \Big(\frac{1}{\mathrm{length}(\tau)} \sum_{\tau=-5s}^{5s} \mathrm{EDTF}_{\mathrm{norm}}(\tau) \Big), \tag{2}$$

where $\mathrm{EDTF}_{\mathrm{norm}}(\tau)$ is the relative EDTF value. This ratio, which is obtained with Equation 2, describes the magnitude of coupling between the signals A and B without any delay compared to the coupling with delay.

In this thesis ASI was measured between the two hemispheres, F3P3–F4P4, as well as between the monopolar channels, F3–P3, F4–P4, F3–F4, P3–P4. This resulted in five different ASI values for every epoch.

3.3.2 Weighted phase lag index

Phase-locking or phase synchrony is the correlation between the phases of two signals. It means that the phase difference between these signals stays fixed, over a certain period of time. This is illustrated in Figure 6. Phase synchrony is regarded as the functional interaction between two distinct areas of the brain [40]. There are different methods for quantifying the phase synchrony, such as phase locking value (PLV). PLV uses the phases of signals to estimate their phase covariance. The following equation is used for computing PLV:

$$\mathrm{PLV} = \frac{1}{N} \left| \sum_{n=1}^{N} \exp(j\theta(t, n)) \right|, \tag{3}$$

where N is the number of samples, j is imaginary unit and $\theta(t, n)$ is the phase difference between the two signals.

It was first introduced by Lachaux et al. [42]. However, PLV has several disadvantages, such as volume conduction, noise and use of common reference. Thus a new measure, called phase lag index (PLI), was developed by Stam et al. [43]. PLI uses the imaginary component of cross-spectrum to estimate phase correlation. Although PLI is less sensitive to volume conduction than PLV, noise still poses a problem for PLI [43]. To further improve PLI's robustness towards volume conduction and noise, Vinck et al. [44] introduced weighted phase lag index (wPLI) in 2011. wPLI weights the PLI by the magnitude of its imaginary component. If the phase difference between the two signals is close to either 0° or 180°, noise can rotate the cross-spectra across the real axis, turning phase lags to leads and vice versa. However, as the imaginary component of the cross-spectrum is 0 with phase differences of 0° and 180°, the weighting makes wPLI less sensitive to noise than PLI. The difference between PLI and weighted PLI is illustrated in Figure 7. To overcome the problem of sample-size bias, Vinck et al.[44] proposed a metric called debiased wPLI.

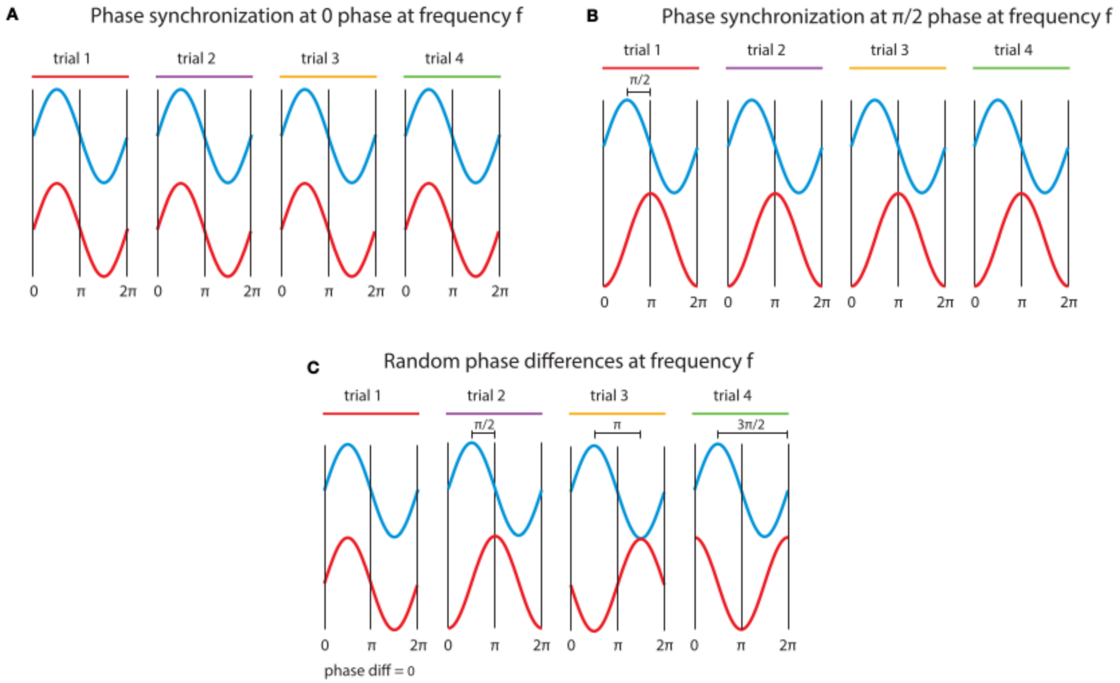

Figure 6: Phase synchrony between two signals (red and blue). (A) Perfect alignment of the phases, phase difference = 0. (B) Perfect synchrony with phase difference of $\pi/2$. (C) Inconsistent phase differences meaning no synchrony. Figure modified from Bastos and Schoffelen[41].

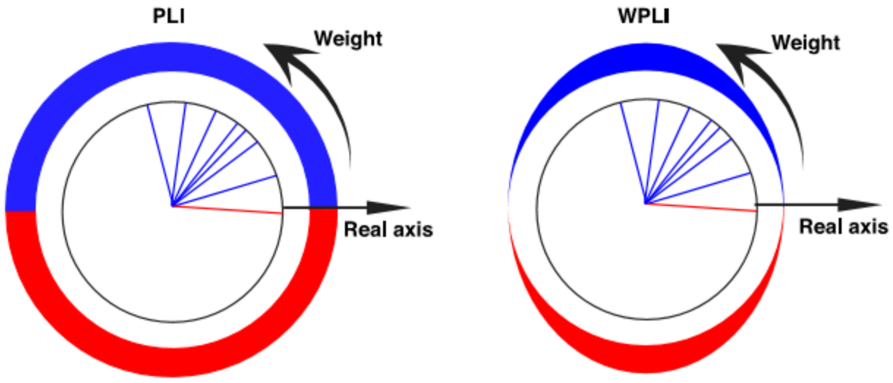

Figure 7: Comparison between PLI and wPLI. All cross-spectra are weighted equally by PLI and assigned a value of either $+1$ or -1, depending on which side of the real axis it lies. $+1$ means phase lead and is illustrated in blue, while phase lag is illustrated in red and assigned a value of -1. wPLI weights the cross-spectra by the magnitude of its imaginary component. Cross-spectra with a real component close to 0 contributes more than cross-spectra around the real axis. Figure modified from Vinck et al. [44]

The first step when computing debiased wPLI is the computation of imaginary components of the cross-spectrum. After the imaginary components have been computed, they are averaged to one value. The computed average is then normalized by the magnitudes of the imaginary components. This results in a following equation:

$$\text{wPLI} = \frac{\sum_{j=1}^{N} \sum_{k=j+1} W_{j,k} d(X_j, X_k)}{N(N-1)\overline{W}}, \tag{4}$$

where $W_{j,k} \equiv |\Im(X_j)\Im(X_k)|$ is the weight, $d(X_j, X_k) \equiv sign(\Im(X_j))sign(\Im(X_k))$, $\overline{W}$ is the normalized weight and $\Im(X)$ is the imaginary component of the cross-spectrum of the respective signal. [44] The wPLI was computed for frequency bands of 0.25–3 Hz, 3–8 Hz, 8–15 Hz and 15–30 Hz and between monopolar channel pairs of F3–P3, F4–P4, F3–F4 and P3–P4. Thus, the total number of wPLI values obtained for every epoch was 16.

3.3.3 Nestedness coefficient

Endogenous burst have been shown to often occur during slow and large voltage deflections in neonatal brain [45]. Nestedness coefficient (NC) is a measure used for estimating this coupling between the phase of slow oscillations and amplitude of faster oscillations within a signal. In other words, this means that the amplitude of the fast oscillations is modulated by the phase of the slow oscillations [46]. Alternatively, the slow oscillation can be phase-locked to the amplitude peaks of the fast oscillations [47]. These nested oscillations have been shown to exist across multiple frequency bands, and possibly play a crucial role in the regulation of large-scale neuronal activities, such as the execution of cognitive functions [45, 46, 48]. In addition, nested oscillations correlate with sensory awareness [49].

In this study the slow oscillations were considered to have a frequency band from 0.2 Hz to 0.6 Hz. The faster oscillations were divided into three frequency bands: 3–8 Hz, 8–15 Hz and 15–30 Hz. For extracting the different frequency bands from the signal, a pair of low-pass and high-pass FIR filters were applied in both forward and backward directions. After filtering, an amplitude envelope for the higher frequency component was obtained with calculating the complex magnitude of Hilbert transformed signal in question. This envelope was afterwards filtered with the same low-pass and high-pass filters used for the lower component. Both the amplitude envelope and the lower component were then extended into complex plane with Hilbert transform. The last step in calculating NC was the computation of PLV, as shown in Equation 3, between these complex signals. In other words, NC thus estimates the phase correlation between the slow oscillating component of the signal and the amplitude envelope of the faster oscillation. Phase-amplitude coupling is illustrated in Figure 8. NC was computed within every monopolar channel and with the three frequency bands, resulted in a total of 12 values for every epoch.

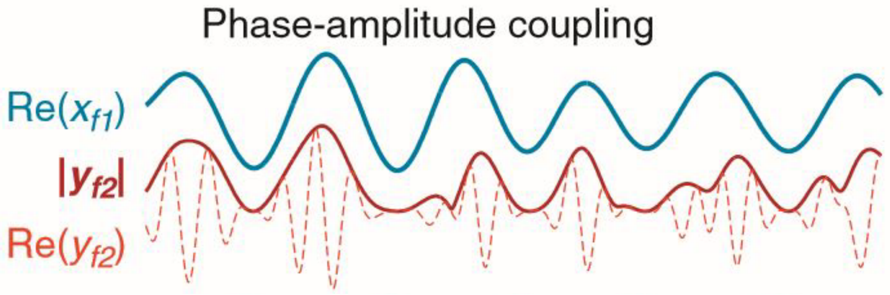

Figure 8: Illustration of phase-amplitude coupling. Phase of the slow oscillation (blue) is correlated with the amplitude of the fast oscillation (red dashed line). Amplitude envelope of the fast oscillation is shown in red solid line. Figure modified from Palva and Palva [49].

3.3.4 Power spectral density

In power spectral density (PSD) analysis the power of the signal is plotted against frequency. Thus, PSD describes how the power is distributed into different frequencies. Attenuation of EEG can be detected with PSD and it has been shown to differ between healthy and sick neonates in a low frequency range close to delta waves [50].

In the studies, Welch's estimate was used to compute the PSD. In this method, the time series is divided into segments, which was chosen to be 10 seconds in length with 50% overlap. After the division into segments, a Hamming window is applied before obtaining modified periodograms from each segment. The periodograms are obtained by computing the fast fourier transforms (FFTs) of autocorrelation functions of the segments. These periodograms are then averaged to reduce variance and an estimate of PSD for the time series is obtained. [51]

A total of four frequency bands were used, specified in Table 1, for which the average power carried over the frequency band were estimated. Averaging was done by taking a mean value of the spectrum to obtain a single value of power per frequency band. An example of a modified periodogram computed from one 5 min long epoch, two subsequent 2.5 min epochs, of one subject can be seen in Figure 9.

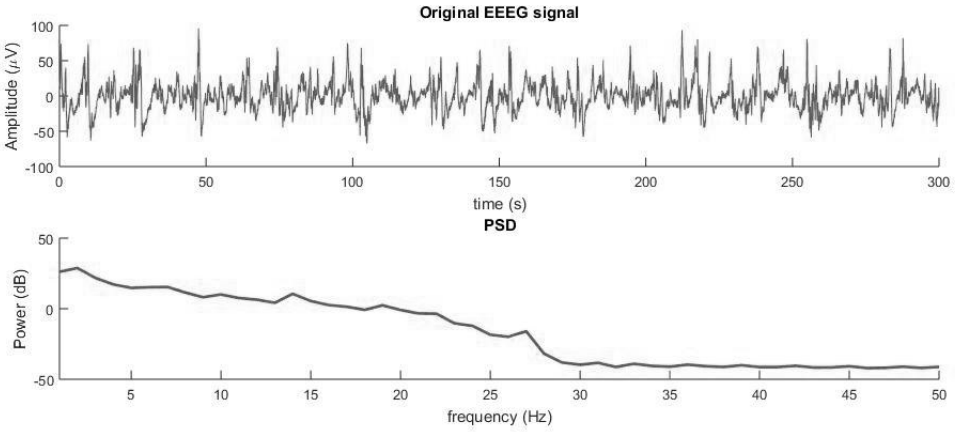

Figure 9: Power spectral density of computed from 5 min epoch of one of the subjects. The original signal is shown above the PSD.

3.3.5 Cross power spectral density

Cross power spectral density (cPSD) is often used in computing the coherence of two signals, which is a measure used to evaluate phase correlation, as is wPLI [41]. However, in our studies we used cPSD to measure the powers of two channels. While PSD estimates the signal power of one channel, cPSD assesses the power per unit frequency shared between two channels.

The computation of cPSD is similiar to the one of PSD with the exception that cross-correlation is used instead of autocorrelation. Thus, cPSD is the FFT of the

cross-correlation of the two signals. Cross-correlation of two signals X_1 and X_2 can be defined as:

$$R_{X_1,X_2}(\tau) = E[X_1(t)X_2(t+\tau)], \tag{5}$$

where τ is the time lag between the two signals. To estimate the cross power spectral densities Welch's estimate was used in the same manner as with PSD. cPSD was computed for the same montage pairs as ASI, as it also is a measure between montage pairs. With the four frequency bands (1–3 Hz, 3–8 Hz, 8–15 Hz and 15–30 Hz), it resulted in 20 different values for every epoch.

3.3.6 Amplitude-integrated EEG

Amplitude-integrated EEG (aEEG) is used for bedside monitoring of neonates for seizure detection and evaluation of the baseline activity of the brain [52]. aEEG can additionally be used for predicting the outcomes of neonates with encephalopathy caused by various reasons [53]. In aEEG the raw EEG recording is first filtered so that frequencies below 2 Hz and above 15 Hz are attenuated strongly. After filtering, the signal is then rectified and smoothed to illustrate the trending. Thus, aEEG is a measure of peak-to-peak amplitude. aEEG is presented in a time-compressed form to illustrate the activity of the brain over longer time periods. [54]

After the computation, two attributes of aEEG were then calculated. These attributes were mean and interquartile range (IQR). These two attributes characterize the different aspects of the value distributions, mean is associated with the central tendency while IQR describes the spread or variability of the distribution [54]. Both of these can be used to analyze the possible attenuation of EEG caused by dexmedetomidine. The appereance of aEEG is illustrated in Figure 10.

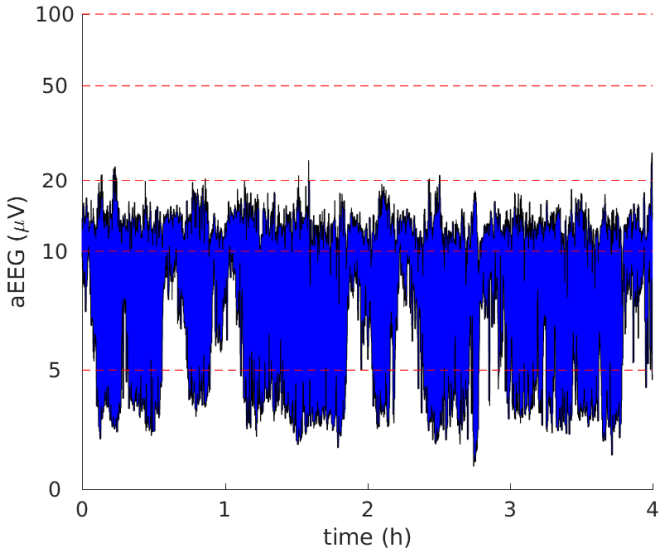

Figure 10: An example of aEEG from one of the subjects. The figure shows one channel of a postdrug recording that has been transformed into aEEG.

3.3.7 Range-EEG

In order to account for the filtering in aEEG and thus underestimation of frequencies either below 2 Hz or over 15 Hz, range-EEG (rEEG) can be used to measure the peak-to-peak amplitudes of EEG. rEEG is calculated as the minimum amplitude substracted from the maximum amplitude for two second windows with no overlap. This corresponds to the high-pass filtering of 0.5 Hz of traditional EEG. [54] On the contrary to aEEG, which is an underestimate of peak-to-peak amplitude, rEEG is an overestimate. This means that the value of rEEG is a little higher than the average peak-to-peak amplitude for a two second window.

The rEEG recordings were cut into 2.5 min epochs without overlap and three different variables were then computed for each epoch. These variables were mean, IQR and lower 5th percentile (LI). LI of rEEG has been proven to increase with the maturation of the brain and its abrupt rises has been associated with epileptic seizures [54, 36]. The appereance of rEEG is illustrated in Figure 11.

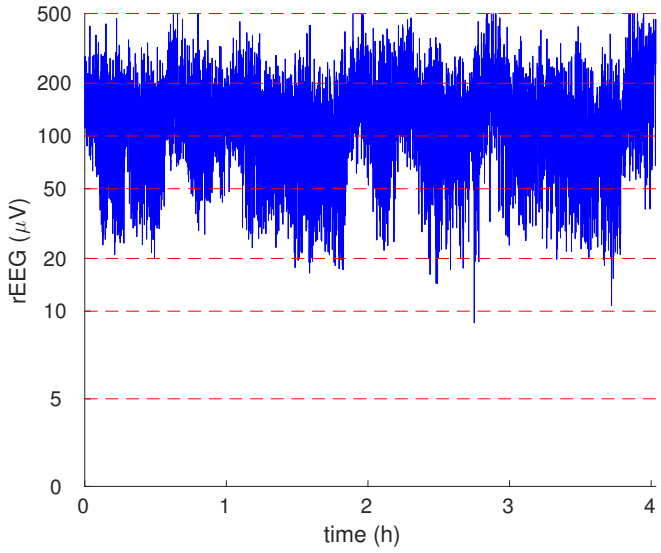

Figure 11: An example of rEEG from one of the subjects. The figure shows the same channel of a postdrug recording transformed into rEEG as with aEEG.

3.3.8 Multifractal detrended fluctuation analysis

Structures or patterns repeating itself over various temporal scales are often found in biomedical signals [55]. One method to assess this self-similarity or fractality is by detrending fluctuation analysis (DFA). If the fractality of the signal is temporally and spatially independent, the structure can be defined by a single singularity exponent and is considered monofractal. However, if a single exponent is not sufficient to express the power-law of the fractality and several are needed, the signal is considered multifractal. DFA has been adapted to multifractal signals, resulting in a method called multifractal detrended fluctuation analysis (MFDFA).

Multifractal analysis has not only been shown to differentiate between different pathological conditions but also between the neural activity of different areas of the brain [56, 57]. Thus, multifractal analysis could serve as a powerful tool in diagnostics.

The computation of MFDFA consisted of five steps, following the work of Kanelhardt et al. [58]. The first step was determining the profile of the signal. This means that the noise like signal is converted into random walk by first subtracting the mean value the signal followed by integration of the time series. This is done in the following equation:

$$Y(i) \equiv \sum_{n=1}^{N} (x_n - \langle x \rangle), i = 1, ..., N. \tag{6}$$

In this equation N is the number of data points and $\langle x \rangle$ is the mean of the signal. In the second step, the profile $Y(i)$ was divided into N_s segments with no overlap and a length of s data points. After the division into segments, local trends for each segments were computed with the usage of a least-square fit. The third step also included determining the variance for each segment v with a length of s by the following equation:

$$F^2(s, v) \equiv \frac{1}{s} \sum_{i=1}^{s} Y[(v-1)s + i] - y_v(i)^2, v = 1, ..., N_s. \tag{7}$$

The fourth step consisted of averaging over all segment in order to obtain the fluctuation function of qth order. The values for index q used in this thesis had a range from -5 to $+5$ with a step size of 0.5, following the work of Matic et al. [59].

$$F_q(s) \equiv \frac{1}{N_s} \sum_{v=1}^{N_s} \left([F^2(s, v)]^{q/2} \right)^{1/q}. \tag{8}$$

The second, third and fourth steps are repeated for different segment lengths in order to assess the dependence between fluctuation functions $F_q(s)$ and time scales. The time scales of s used in this work had a range from 25 to 1875 samples, 1875 samples fitting twenty times into a 2.5 min epoch with a sampling frequency of 250 Hz. The smallest scale of 25 samples was determined, following the instructions found in the work of Ihlen at al. [55]. The number of scales in total was 19 and they were determined by equidistant spacing in logarithmic scale between $\log_2(25)$ and $\log_2(1875)$.

The fifth and final step was to determine the scaling behaviour of the fluctuation functions $F_q(s)$. The relation between the fluctuation functions and scales is shown in the following equation:

$$F_q(s) \sim s^{H(q)}. \tag{9}$$

The scaling behaviour was determined by analyzing plots of $F_q(s)$ against different scales of s in logarithmic scale with different values of q. An example of these plots is shown in Figure 12. The slopes of these plots are q-order Hurst exponents, $H(q)$. The q-order Hurst exponents can be used to determine both the q-order singularity exponent $h(q)$, as well as the q-order singularity dimension $D(q)$:

$$h(q) = H(q) + qH'(q) \quad \text{and} \quad D(q) = q[h(q) - H(q)] + 1. \tag{10}$$

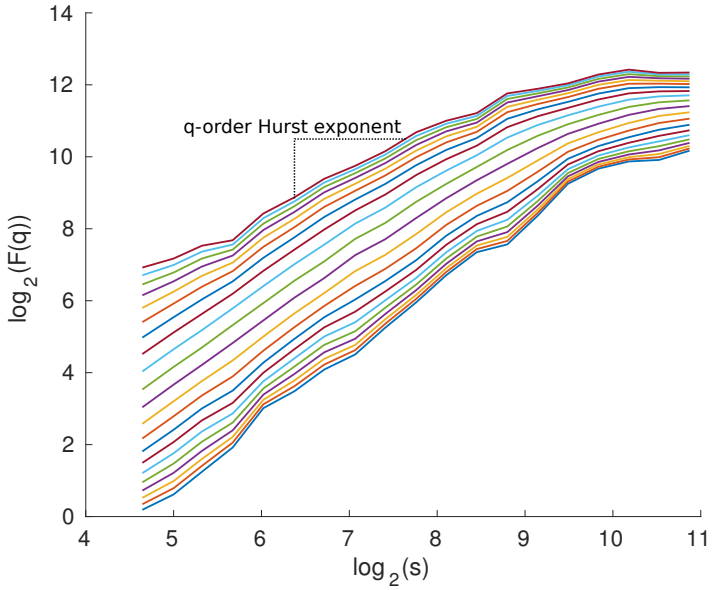

Figure 12: An example of q-order fluctuation $F(q)$ plotted against different scales of s in logarithmic scale. Different values of q are plotted in their own lines, of which slope is the respective q-order Hurst exponent.

A multifractal spectrum can be obtained by plotting the $D(q)$ against the singularity strength $h(q)$. An example of multifractal spectrum is shown in Figure 13. Out of the multifractal spectrum, four variables were extracted that describe the spectrum. These variables were *width hq*, *height Dq*, *peak hq* and *tail Dq*. While the two first measures are related to the size of the spectrum, *peak hq* and *tail Dq* describe the asymmetry of the spectrum. Both *width hq* and *height Dq* were computed following work of Zorick and Mandelkern [60]. *Width hq* is the difference between the maximum and minimum $h(q)$ values. *Height Dq* describes the temporal changes in the local Hurst exponents and is defined as the minimum $D(q)$ subtracted from the maximum $D(q)$. *Peak hq* is the singularity exponent $h(q)$ where the singularity dimension $D(q)$ reaches its maximum. The last variable, *tail Dq*, describes whether the multifractal spectrum has a longer tail either with smaller or larger values of $h(q)$. A left tail refers to a longer tail with smaller values of $h(q)$ (negative *tail Dq*), while right tail stands for a longer tail with larger values (positive *tail Dq*).

Tail Dq was computed as the difference between the $D(q = 5)$ and $D(q = -5)$. *Tail Dq* was first introduced by Matic et al. [59]. All of these variables are illustrated in Figure 13.

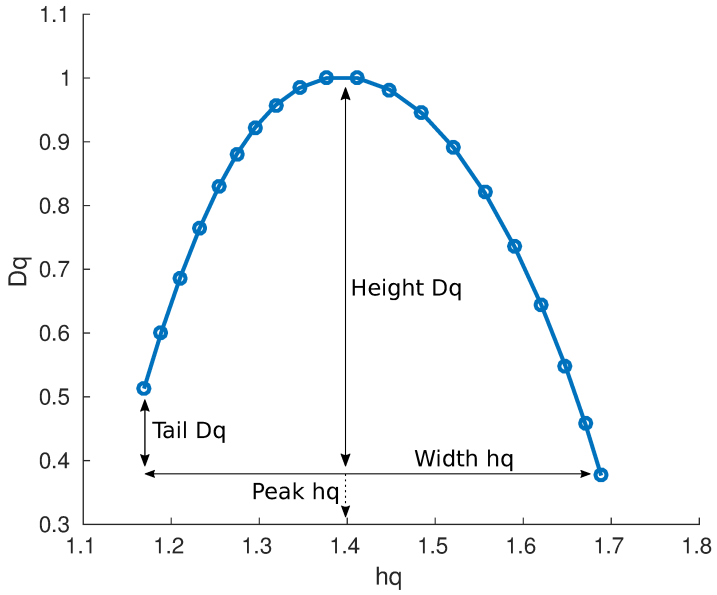

Figure 13: An example of multifractal spectrum from one of the subjects. The four different measures computed that describe the spectrum are shown.

3.4 Statistical methods

In this section, the methods used for the statistical analysis of the gathered feature values of EEG are introduced. As all of the pre- and postdrug feature comparison are related, meaning we have pairs of values, Wilcoxon signed-rank test was used for analysis. When the results were independent from each other, Wilcoxon rank-sum test was used. With the results grouped in more than two groups, Kruskal-Wallis one-way analysis of variance was applied. All of the used tests were thus non-parametric, meaning that no assumptions of the distributions were made.

3.4.1 Wilcoxon signed-rank test

Wilcoxon signed-rank test is a statistical method used to compare two samples that are paired. In this test, the two distributions of samples are not assumed to follow normal distributions. In Wilcoxon signed rank test, first the differences between the pairs are calculated as $|x_i - x_j|$, where x_i and x_j are the related pair of values. These differences are then assigned a rank value, based on their magnitude. The sign of the differences, $\text{sign}(x_i - x_j)$ is also applied to the ranks. For example, differences of 1, 3 and -6 would be receive ranks of 1, 2 and -3 in respective. [61] A test statistic W of Wilcoxon signed-rank test is the sum of these signed ranks.

From the test statistic, a z-score can then be calculated as:

$$z = \frac{W}{\sigma_W}, \sigma_W = \sqrt{\frac{N(N+1)(2N+1)}{6}}, \tag{11}$$

where σ_W is the standard deviation of W and N the number of pairs.

This z-score is then compared to a z-distribution, in order to obtain a p-value for the test. The null hypothesis for Wilcoxon signed-rank test is that the differences of the two samples follow a distribution, which has a median of zero. The tests p-value is the probability of observing a value greater than or equal to the calculated test statistic. [62] Based on the p-value and a chosen level of confidence, the null hypothesis either holds or is rejected. In the statistical analyses performed in this thesis, the chosen confidence level was 0.05 and p-values less than or equal to 0.05 meant the rejection of the null hypothesis.

3.4.2 Wilcoxon rank-sum test

Wilcoxon rank-sum test was used when the observations were not paired. It is a statistical method for testing the equality of medians between two groups. In Wilcoxon rank sum test, the two groups of samples are merged together and every sample is assigned a rank based on its magnitude. Unlike in the signed-rank test, only positive ranks are assigned and the sign of the sample is neglected. A test statistic W is then calculated as the sum of ranks of the first group. With large enough sample sizes, a z-statistic can then be used to compute the p-value of the test. The z-statistic in Wilcoxon rank-sum is defined as:

$$z = \frac{W - E(W)}{\sigma_W}, \tag{12}$$

where $E(W)$ is the expected value of the test statistic W and σ_W is its standard deviation.

As with the Wilcoxon signed-rank test, the Z-statistic is then compared to z-distribution for obtaining an approximation of the p-value. The selected level of significance was 0.05 in all of the Wilcoxon rank-sum tests. [61, 62]

3.4.3 Kruskal-Wallis test

Kruskal-Wallis tests the null hypothesis that all the values of different groups come from the same distribution. An often used method for the same problem is the F-test that assumes that all the distributions are normally divided, however, no such assumption is made with Kruskal-Wallis. It can be used for three or more groups and the sizes of the groups do not have to be equal. [63]

In Kruskal-Wallis, null hypothesis is tested by ranking the samples of all the groups from 1 to N and calculating H statistics. By using the ranks instead of actual values, the calculations are simplified and only general assumptions, such as symmetry of the distribution and independence of the samples, are made.

If two or more observation have the same value, they are replaced by the mean of their supposed rankings. H-test is defined by:

$$H = \frac{12}{N(N+1)} \sum_{i=1}^{C} \frac{R_i^2}{n_i} - 3(N+1), \tag{13}$$

where C is the number of groups, N is the number of observation in all C groups combined and R_i is the sum of the ranks in a group i.

For large enough number of observations, value H is then compared with the χ^2-distribution, which is the sum of squared errors with the degree of freedom being the number of groups, C. If H is larger than $\chi^2(C-1)$, the null hypothesis is rejected. Kruskal-Wallis is one-way variance analysis and it compares the medians between each group. This test does not tell which two groups differ significantly, only that some of them do or none of them do not.

3.4.4 Spearman's rank correlation

Spearman's rank correlation is a nonparametric measure for the dependence of the ranks of two samples. When computing Spearman's rho, the two samples are first ranked separately based on their magnitude while keeping the observation pairs intact. Pearson's correlation coefficient is then calculated for these n pairs of ranks. [62] Spearman's rho is defined as:

$$r_s = \frac{\sum_{i=1}^{n}(x_i - \overline{x})(y_i - \overline{y})}{\sigma_x \sigma_y}, \tag{14}$$

where x_i and y_i are the ranks of the i^{th} pair of observations. Moreover, $\overline{x}$ and $\overline{y}$ are the means of ranks of the two samples. σ_x and σ_y represent the standard deviations of the two ranked samples and n is the number of pairs.

If there are no ties between the ranks in the samples, Spearman's rho can be simplified to:

$$r_s = 1 - \frac{6\sum_{i=1}^{n} D_i^2}{n(n^2-1)}, \tag{15}$$

where D_i is the difference between the ranks of the i^{th} pair, $D_i = x_i - y_i$. [62]

As Spearman's rank correlation is calculated with ranks instead of actual values of the observations, it is more resistant towards outliers than Pearson's correlation. The correlation coefficient gets values between -1 and $+1$, so that -1 equals perfect negative correlation, 0 means no correlation and $+1$ is perfect positive correlation. Although, a correlation could be strong, it is not necessarily significant. Thus, a p-value evaluating the significance of the correlation can be estimated by first calculating a t-value defined as:

$$t = r_s \sqrt{\frac{n-2}{1-r_s^2}}, \tag{16}$$

where $n - 2$ is the degree of freedom. This t-value is then compared to Student's t distribution in order to determine the corresponding p-value. [64]

3.5 Different studies

In order to study the effects of dexmedetomidine, different studies were conducted. These studies were design to reveal information regarding both the hour long effects of dexmedetomidine, reffered to as time trends from here on, and the short-term effects. In addition, the effect of the EEG state of the subjects before receiving the drug on the effects of dexmedetomidine was investigated. In order for a more thorough study, also different factors that might affect the features values before dexmedetomidine were examined.

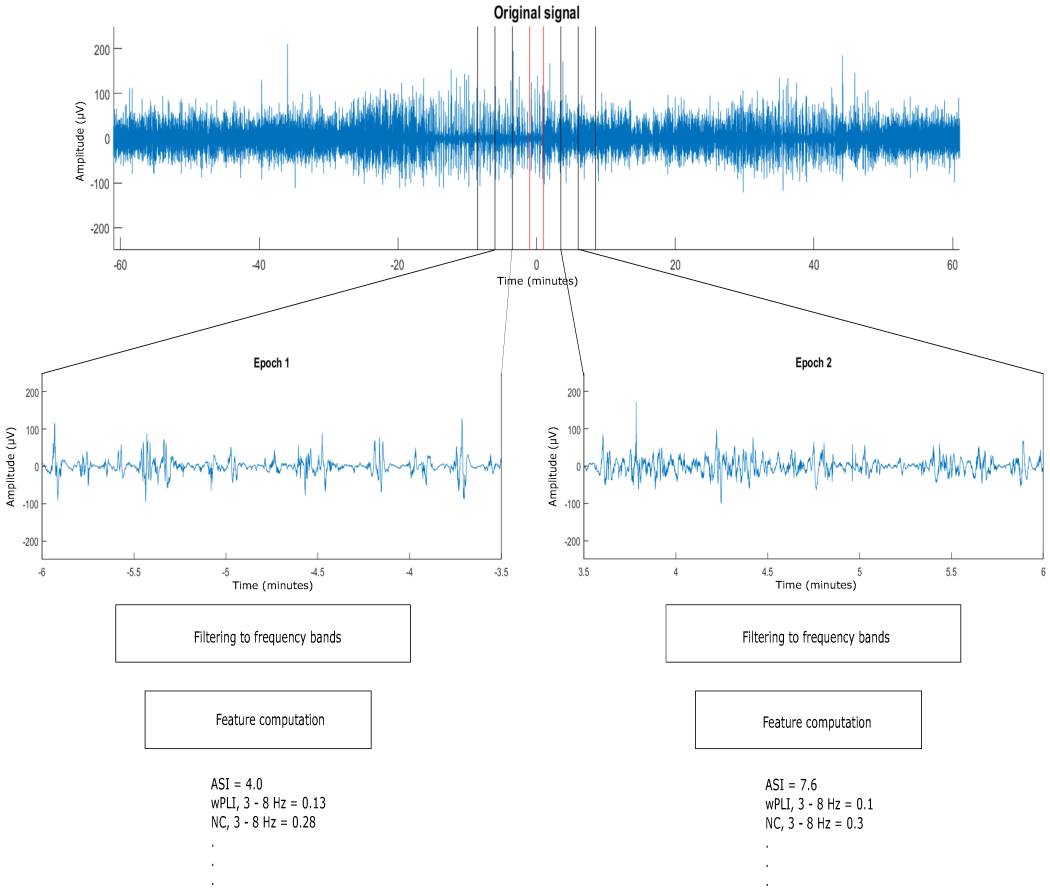

Figure 14: Presentation of how the signal was first divided into 2.5 min long epochs after which the features were computed for every epoch. Time 0 is when the subject received dexmedetomidine. Red vertical lines in the top most picture are 1 min margins while black vertical lines present the epochs. Unlike illustrated in this figure, the whole length of the original signal was cut down into 2.5 min epochs.

3.5.1 Time trends

First, the time trends of all the features were analyzed by dividing all of the records into 2.5 min long epochs and calculating the features for each epoch. As the recordings could not be divided evenly in to 2.5 min epochs, the excess data at the start of the predrug recordings and at the end of the postdrug recordings was cut. From the feature values of each subject for every montage and frequency band, a mean was calculated to measure the time trend of the feature in question. These means of each epoch were then plotted as a function of time to visualize the dynamics of the features over time. Additionally, to provide a more robust estimation of the time trends, means for 10 min epochs with 50% overlap were calculated as a mean of four subsequent 2.5 min epochs. For features that used separate frequency bands, the low frequency artifact masks were applied for frequency bands that included frequencies from 0.15 Hz to 0.5 Hz. If the low frequency artifact mask indicated that an epoch contained more than 10% of artifacts, the whole epoch was rejected. The high frequency masks were applied in the same manner as the low frequency masks, when the frequency band included frequencies from 15 Hz to 25 Hz. For features that did not use specific frequency bands, both the low and high frequency masks were applied. For artifacts detected with the amplitude-based detector, the same threshold of 10% per epoch was used. If the 2.5 min epoch contained more than 15 seconds of artifacts, the whole epoch was rejected. The calculated time trends were then plotted and inspected visually to detect clear prominent changes in the feature values after the patients had received the drug.

3.5.2 Short-term effects

In addition to studying the effects of dexmedetomidine from the complete recordings, the short-term effects were also examined. In this study the feature values of a 10 min epoch after the patients received the drug were compared to a baseline value that was calculated from a 12 min epoch before the drug. The 10 min epoch will be referred as DX and the baseline epoch as BL from here on.

Originally the BL had a length of 10 min as well. However, as some of the predrug recordings had an excessive amount of artifacts, prolonging BL to 12 min increased the number of feature values that were able to be computed. Making the baseline epoch longer than 12 min did not increase the number of feature values obtained when compared to the 12 min epoch. Both the DX and BL had a one min margin from the point when the patients received the drug.

From these epochs, artifacts were first removed and then the remaining data concatenated. The artifact free signals were then cut down into 2.5 min long windows, for which the features were calculated. As the maximum number of windows for the baseline and the DX epoch was 4, a median was used to calculate a single value both of the epochs. If there were less than two and a half min remaining of the data, the feature was ignored. These results were then compared with Wilcoxon signed-rank test. An example of the comparison between DX and BL values can be seen in Figure 15.

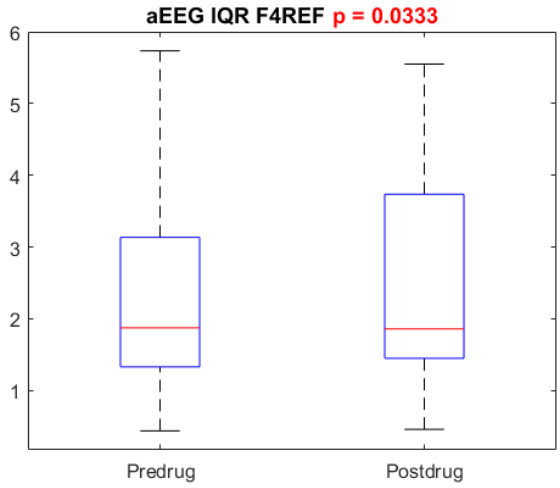

Figure 15: An example illustration of pre- and postdrug values of the interquartile range of aEEG in channel F4. The red line within the boxes represents the mean value of the pre- or postdrug group. P-value in the title is for Wilcoxon signed-rank test.

As it could be hypothesized that the expression of the drug effect in EEG could be dependant on the state of EEG when the subject received the drug, another study with the BL and DX values was conducted. In other words, the predrug value of the feature could have an effect on how the feature value changes as the drug is given. We studied this relationship by making a scatter plot of the absolute change against the BL value. The change between the post- and predrug values will be addressed as delta values from here on. A Spearman's correlation coefficient was then calculated for these two groups, delta and baseline values, to access the correlation between them. The delta values of wPLI in channel F3–F4 and frequency band from 8 to 15 Hz are plotted against the baseline value as an example in Figure 16a. Another way to present this correlation between the delta and the baseline values can be seen in Figure 16b.

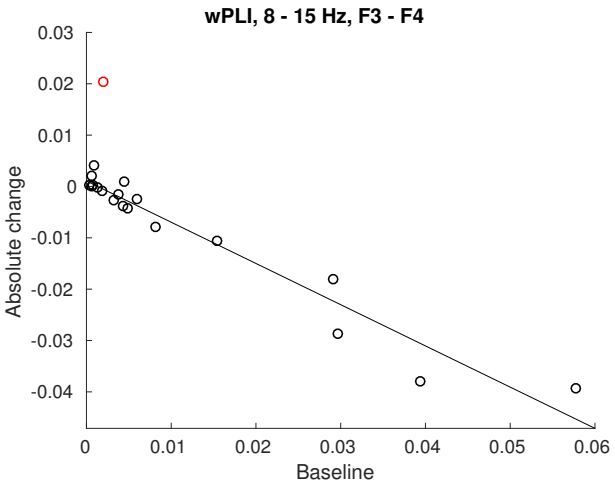

(a) Example plot of how the correlations were analyzed and plotted in this study.

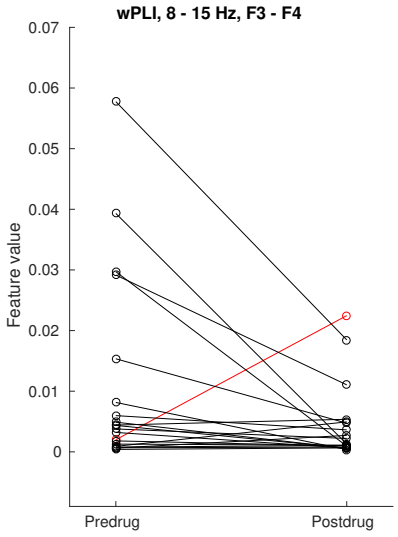

(b) An alternative representation, where the negative correlation could be interpreted.

Figure 16: Correlation between the delta and baseline values of wPLI channel F3–F4 in frequencies from 8 to 15 Hz. (a) scatter plot of the deltas and baseline values (b) Pre- and postdrug values, where the values of the same subject are connected with a line. In both figures, an outlier subject whose feature value actually increased is highlighted in red. The correlation coefficient was -0.580 with the p-value being smaller than 0.000.

3.5.3 Clinical factors

As the baseline value could impact the postdrug value of the same feature, we chose to study several factors possibly affecting the baseline value. The three different factors studied were fentanyl, given to a part of the subjects, conceptional age and background diagnosis. If these factors affected the baseline, it could possibly fade out the effects of dexmedetomidine and alter the results found.

Fentanyl is a drug used for anesthesia or analgesia that affects the central nervous system and could possibly have an effect on EEG as well. Out of all of the 21 subjects, 12 had received fentanyl. The effect of fentanyl on the baseline was analyzed with Wilcoxon's rank sum test to find out if there were differences in the baseline values between the subjects that had received the drug and the ones that had not. An example boxplot where fentanyls effect on nestedness coefficient is plotted, can be seen in Figure 17.

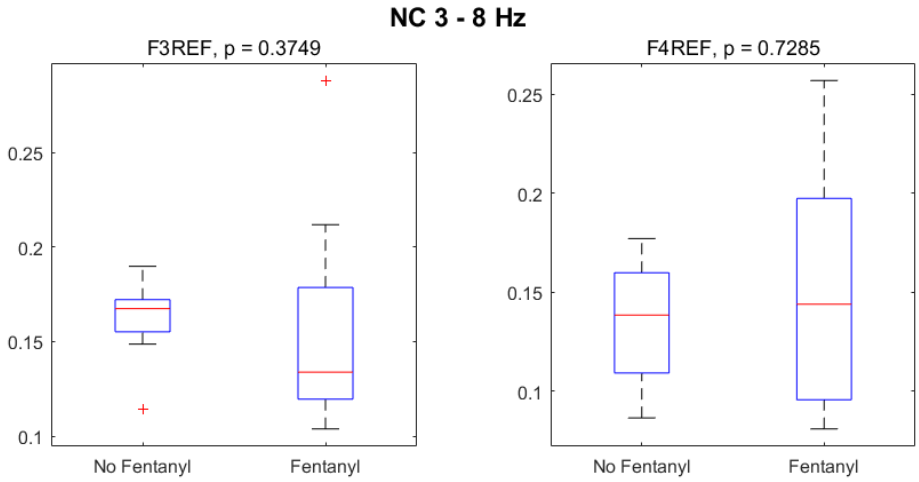

Figure 17: An example illustration of the effect of fentanyl on the baseline value of nestedness coefficient in 3–8 Hz frequency band for each montage.

The second factor, conceptional age, is the age of the neonate calculated from conception. As stated previously, the conceptional ages of the subjects ranged from 197 up to 306 days. Due to the rapid development of neonatal brain, conceptional age could be hypothesized to correlate with at least some of the features used in the studies. For assessing the correlation between the conceptional age and the baseline, Spearman's correlation test was used. In Figure 18, example scatter plots on conceptional ages effect on ASI are presented.

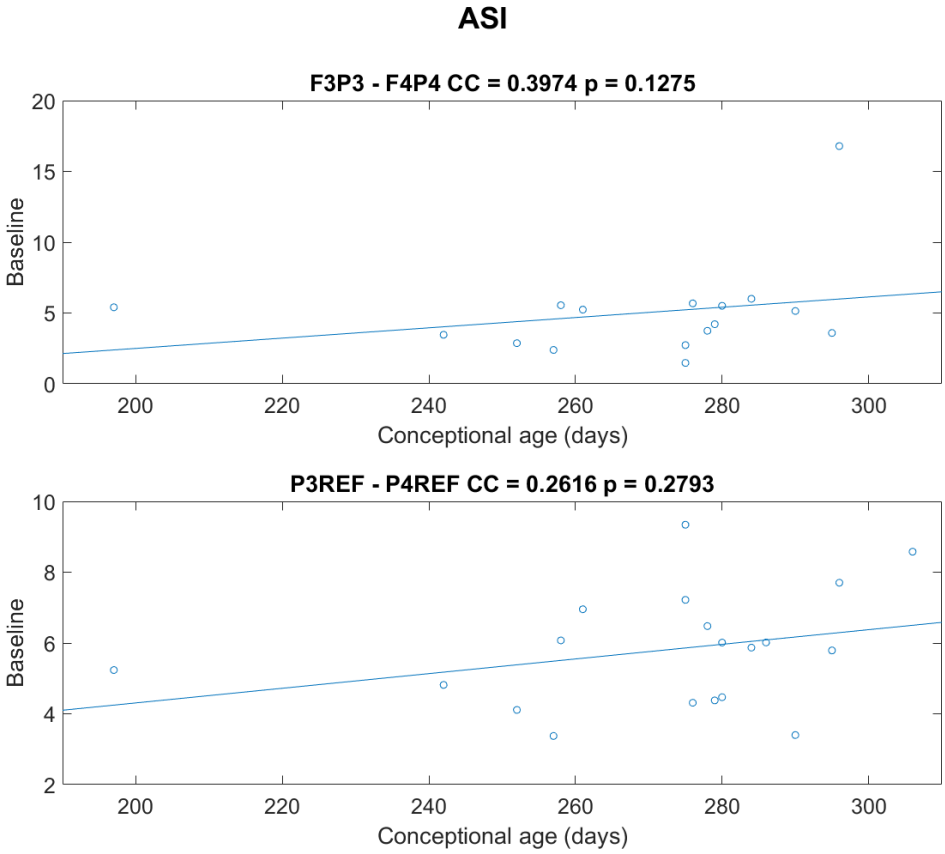

Figure 18: An example illustration of conceptional ages effect on ASI of the baseline for each montage. Figure shows individual subjects as circles and a least squares line. As can be seen, conceptional age does not show correlations with ASI in these two montages. In the title CC stands for correlation coefficient.

The background diagnoses consisted of four different categories, based on their main diagnoses. These groups were:

0 = other

1 = mild or moderate HIE

2 = severe HIE

3 = myocardial infarction or intraventricular hemorrhage

HIE is brain damage caused by the loss of oxygen or deprivation of blood circulation. This in turn can affect the cortical activity of the neonates. Five subjects were diagnosed into group 0, while groups 1 and 2 had eight and six subjects, in respective. Only two subjects were assigned into group 3. The last factor was examined with Kruskal-Wallis test to find out whether the groups of baseline values come from the same distribution or not. Examples boxplots of the background diagnosis affecting the baseline are shown in 19.

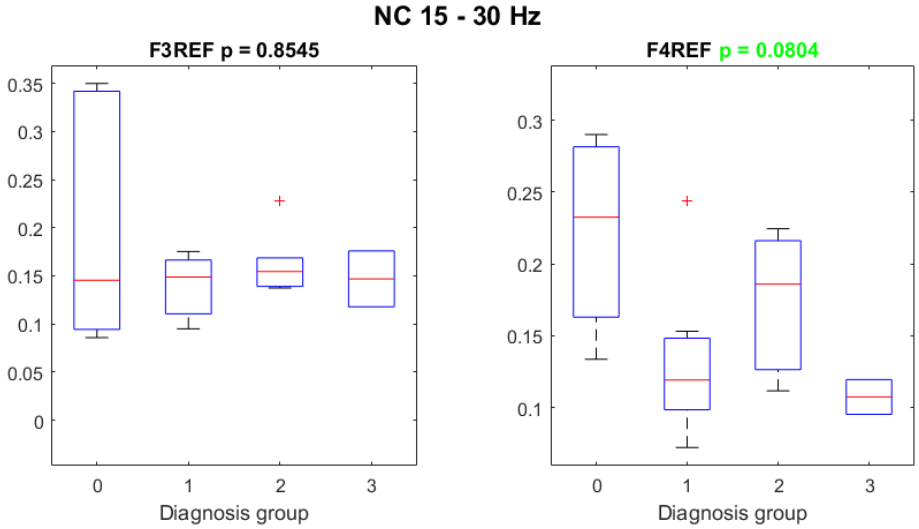

Figure 19: An example illustration of the severity of the diagnosis effect on the baseline value of nestedness in 15–30 Hz frequency bin for channels F3 and F4. Diagnoses are plotted in different boxplots.

4 Results

The results for the different studies introduced previously are presented in this section. In addition, correlations between different features are assessed at the end of this section. As the number of feature vectors and studies were large, only significant results and examples are presented and all of the gathered results for statistical tests can be found in the tables of Appendix A.

4.1 Time trends

The total number of time trends plotted in this study was 125, with all of the different frequency bands and channels listed in Table 1. All of the time trends were evaluated visually with the emphasis being on clear systematic changes in the postdrug feature values, such as notable increases or decreases.

None of the time trends of features analyzed showed any clear changes. Some minor fluctuations were apparent in most of the features, however, the fluctuation did not seem to either increase or decrease after the subjects had received the drug. On the contrary, the fluctuations were rather arbitrary through out the recordings in these cases. An example of time trend plot of ASI is presented in Figure 20. However, it should be noted that for illustration only the 200 minutes around the dexmedetomidine dosing is shown. For the visual analysis the whole length of 480 minutes, for most subjects, was used.

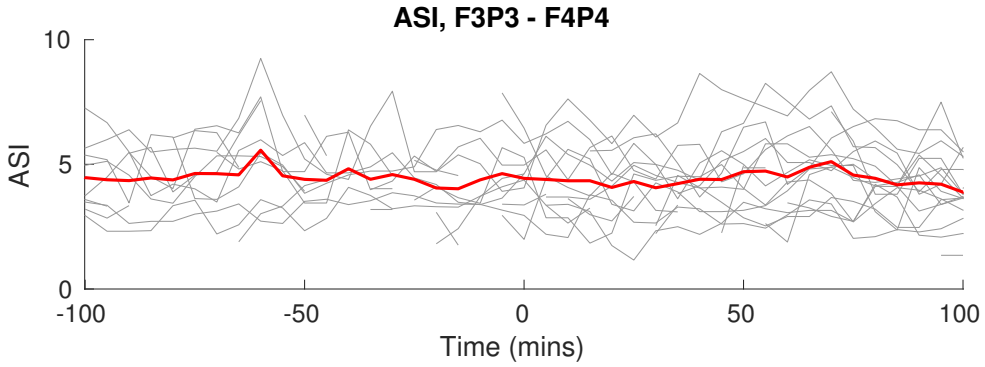

Figure 20: Time trend of ASI for channel F3P3–F4P4. In the figure, subjects are plotted in grey while the red plot is the mean of 10 minute epochs of all subjects. As can be clearly seen from the figure, the mean values showed no clear effects of dexmedetomidine.

4.2 Short-term effects

The second study was about the short-term effects of dexmedetomidine. As previously mentioned, this study included the Wilcoxon signed-rank test between the values before and after the administration of the drug. Another part of this study was the computation of Spearman's rank correlation between the delta and the baseline values. Compared to the time trends study, two additional features were added

for assessing the short-term effets. The features added were the MFDFA measures and lower index of rEEG.

ASI: No significant differences between the pre- and postdrug values for ASI. However, the changes in the values of ASI had significant correlations with the delta and baseline values as the bipolar montage pair F3P3–F4P4 and both the F4–P4 and F3–F4 had a p-value less than 0.05. All of these correlations were negative, with correlation coefficients of −0.753 for F3P3–F4P4, −0.548 for F4–P4 and −0.496 for F3–F4. This means that the greater the value of ASI before the drug, the greater the decrease after the drug was received. The correlation between delta and baseline values in F3P3–F4P4 can be seen from a scatter plot presented in Figure 21c.

wPLI: With wPLI, only F3–F4 in a frequency bin from 8 Hz to 15 Hz had a significant difference between the pre- and postdrug values. However, 9 out of 16 from all frequency bins and channel pairs had significant correlations between the delta and baseline values. The channel pair F3–P3 showed significant correlations in both frequency ranges of 0.25–3 Hz and 3–8 Hz. For F4–P4 the frequency ranges that had significant correlations were 8–15 Hz and 15–30 Hz. The third channel pair, F3–F4, had significant correlations in 0.25–3 Hz, 3–8 Hz and 8–15 Hz ranges. The posterior channel pair P3–P4 showed significant correlations in frequencies from 3 to 8 Hz and 15 to 30 Hz. Moreover, as with ASI, they all had strong negative correlations, with the correlation coefficients ranging from −0.462 to −0.839. A few examples of significant correlations between the delta and baseline values of wPLI can be seen in Figures 21a and 21b.

NC: Nestedness did not show any significant differences between the comparison of postdrug and BL values. This means that the null hypothesis of the Wilcoxon signed-rank test held in all of the frequency bin and channel combinations. On the other hand, the delta and baseline values in channel F4 had a significant negative correlation across all frequency bins. The Spearman's rank correlation coefficients for these correlations were from −0.46 to −0.746.

PSD & cPSD: The spectral density measures, PSD and cPSD, had only a few significant correlations between the feature delta and baseline values. The strong significant correlations for PSD were in channel F3F4 with a frequency bin from 1 Hz to 3 Hz, as well as channels F3F4, F3 and F4 in a frequency range of 8–15 Hz. For cPSD, most of the significant correlations were in the same frequency bin as with PSD, from 8 to 15 Hz. In this frequency bin, channel pairs that had significant correlations were F3P3–F4P4, F3–P3 and F3–F4. In addition, channel pair F3–F4 showed significant correlation in frequency range of 3–8 Hz. As with all of the previous features, all of these correlations were strongly negative with correlation coefficients ranging from −0.492 to −0.729. In the comparison between the post and predrug values, PSD had no significant results and cPSD had only one. The only significant difference in the pre- and postdrug values with cPSD was the negative correlation, correlation coefficient of −0.367, in the channel pair F4–P4 in a frequency range of 1–3 Hz.

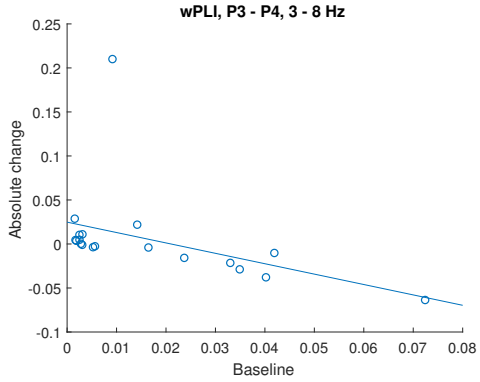

(a) The correlation coefficient between delta and baseline values is −0.753 with a p-value of less than 0.000.

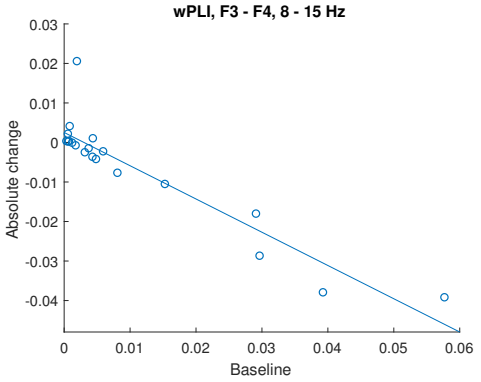

(b) The correlation coefficient between delta and baseline values is −0.580 with a p-value of less than 0.000.

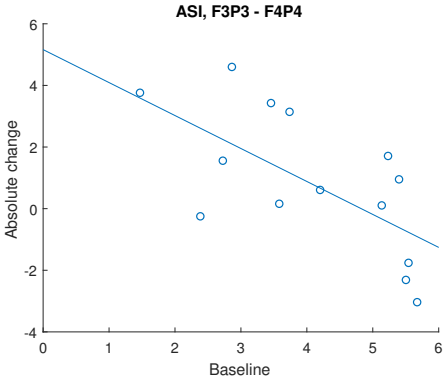

(c) The correlation coefficient between delta and baseline values is −0.753 with a p-value of 0.001.

Figure 21: Scatter plots of delta and baseline values of wPLI montages P3–P4 in 3–8 Hz (a) and F3–F4 in 8–15 Hz (b). Also a significant correlation in ASI montage F3P3–F4P4 is shown in (c).

aEEG: Out of the two aEEG measures, mean and IQR, only the postdrug values of IQR in channel F4 differed significantly from the predrug values. The p-value for Wilcoxon signed-rank test in this channel was 0.033. For correlations between the delta and baseline values, neither mean or IQR showed significant correlations.

rEEG: As with aEEG, the rEEG measures had only a few significant results. These results were the strong negative correlations between the delta and baseline values with the mean of rEEG in channels F3 and P4. Both the IQR as well as the lower index, had neither significant correlations with delta and baseline or differences in the pre- and postdrug distributions of the measure values. Figure 22 shows the scatter plots of rEEG mean values in channels P3P4, F3 and F4. In addition, scatter plot of delta and baseline values in channel F3 of rEEG LI is presented in Figure 25b.

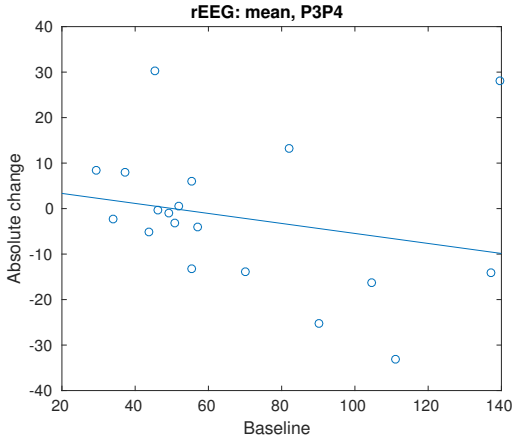

(a) The correlation coefficient between delta and baseline values is −0.414 with a p-value of 0.079.

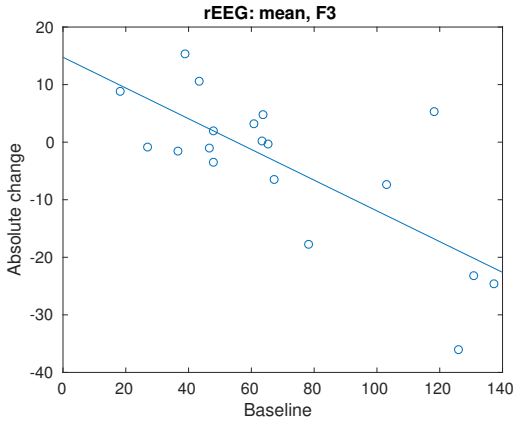

(b) The correlation coefficient between delta and baseline values is −0.612 with a p-value of 0.006.

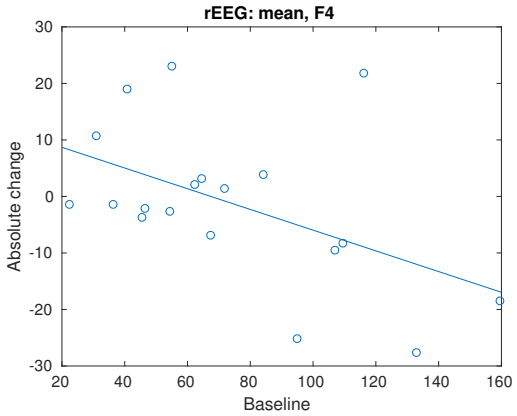

(c) The correlation coefficient between delta and baseline values is −0.440 with a p-value of 0.061.

Figure 22: Scatter plots of rEEG mean values in channels (a)P3P4, (b) F3 and (c) F4.

MFDFA: The last four measures were the *peak hq*, *width hq*, *tail Dq* and *height Dq* of MFDFA. Only *width hq* and *tail Dq* had significant differences between the delta and baseline values. Moreover, both of these measures had significant differences only within one channel. These channels were F3F4 for *width hq* and P3P4 for *tail Dq*. However, both *width hq* and *height Dq* showed strong significant correlations between the delta and the baseline values, and as with the previous features, they were all negative with correlation coefficients ranging from -0.486 to -0.728. The channels that showed correlations for *width hq* were F3P3, F3, P3 and P4. For *height Dq*, channels F3F4 and F4 were the only channels that did not show significant correlations. *Tail Dq* had significant correlations in P3P4 and F3 with the coefficients of -0.566 and -0.565, in respective. *Peak hq* showed no significant correlations between the delta and baseline values.

4.3 Clinical factors

For verifying that the results found in the previous studies were indeed a result of dexmedetomidine, various factors that could affect the baseline values were examined. As explained in the methods, the examined factors were whether the subjects had received fentanyl or not, conceptional age and the background diagnosis. The effect of baseline factors were studied with the same features that were used for determining the short-term effects.

ASI: Overall, the listed factors did not affect the baseline values of ASI, with the only exception being a significant difference between the baseline values with subjects that had received fentanyl and with subject that had not. This difference was in channel pair F3P3–F4P4. The channel pair in question also had the strongest negative correlation between delta and baseline values. Figure 23 shows the correlation between delta and baseline values of ASI in this channel, where the fentanyl groups are plotted differently.

wPLI: As with ASI, there was only one significant effect of fentanyl in wPLI. The channel pair that had a significant difference in the fentanyl and non-fentanyl values was F3–P3 in the frequency range of 3–8 Hz. The channel in question also had a strong correlation between delta and baseline values in the same frequency range. In Figure 24 this correlation is presented with fentanyl groups. Conceptional age showed significant correlation also in one channel pair. The channel pair in question was F3–F4 in frequency range of 0.25–3 Hz and had a correlation coefficient of 0.577. The different background diagnoses showed no effect on the baseline values of wPLI.

NC, PSD, cPSD, aEEG & rEEG: The baseline factors had no significant effects for nestedness coefficient, PSD, cPSD or any of the aEEG and rEEG measures, with the only exception being the channel F3 with rEEG LI. The rEEG LI values in F3 had a strong positive correlation with the baseline value and conceptional age of the subject. Although not significant with p-values greater than 0.05, channel F4 of rEEG LI had p-values close to 0.05 in both the delta and baseline study as well as fentanyl study. This is shown in Figure 25a.

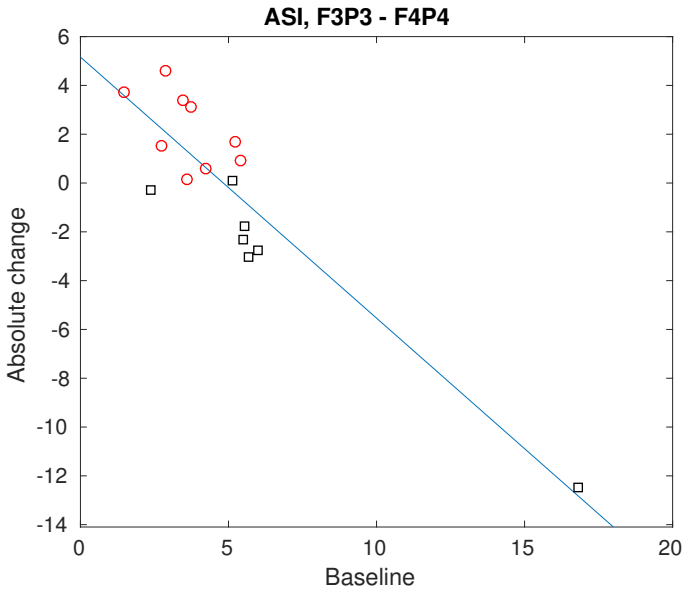

Figure 23: Correlations between the delta and baseline values of ASI in channel pair F3P3–F4P4. Subjects who had received fentanyl are plotted in red circles, while the black squares represent subjects without fentanyl. For illustrating the correlation, a least square fit was plotted in blue. The Spearman's rank correlation coefficient was -0.75 and the respective p-value $= 0.001$. The values of subjects with and without fentanyl have clearly grouped into distinct groups, as the p-value of 0.023 for Wilcoxon rank-sum test would suggest.

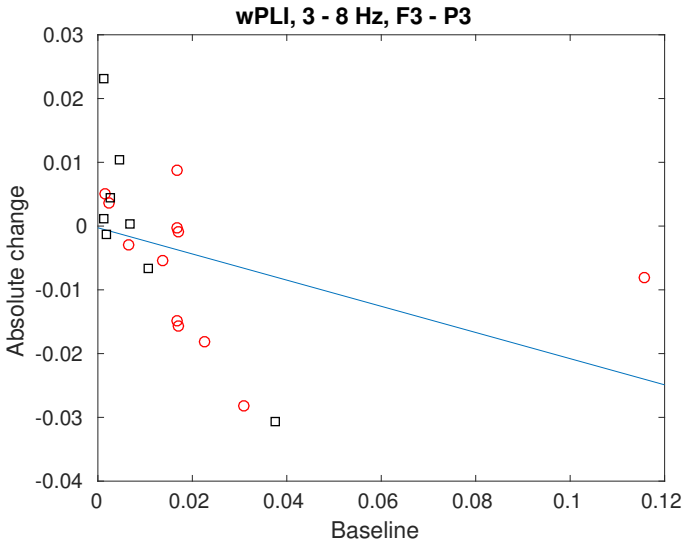

Figure 24: Correlations between the delta and baseline values of wPLI in channel pair F3–P3. Subjects who had received fentanyl are plotted in red circles, while the black squares represent subjects without fentanyl. For illustrating the correlation, a least square fit was plotted in blue. The Spearman's rank correlation coefficient was -0.84 and the respective p-value $= 0.0001$. The corresponding p-value of Wilcoxon rank-sum test for determining the effect of fentanyl was 0.049.

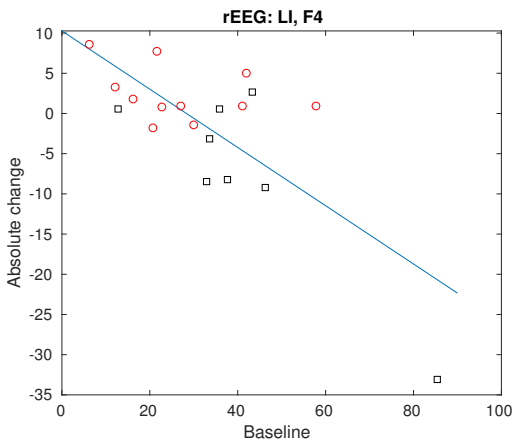

(a) The Spearman's rank correlation coefficient was -0.43 and the respective p-value $= 0.069$. The corresponding p-value of Wilcoxon rank-sum test for determining the effect of fentanyl was 0.091.

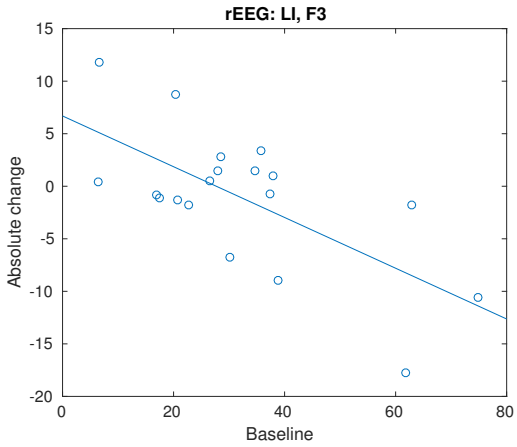

(b) The correlation coefficient between delta and baseline values is -0.447 with a p-value of 0.056.

Figure 25: Scatter plots of rEEG LI values in channels (a) F4 and (b) F3. Correlations between the delta and baseline values of rEEG LI in channel F4. In (a), subjects who had received fentanyl are plotted in red circles, while the black squares represent subjects without fentanyl. For illustrating the correlation, a least square fit was plotted in blue to both figures. Although, neither had a p-value less than 0.05, they were both close to the confidence level.

MFDFA: Out of all of the MFDFA measures, only one showed any effect of fentanyl on the baseline value. The effect of fentanyl was expressed in channel P3 with *height Dq*. On the other hand, conceptional age showed significant correlations in most of the channels with *peak hq*. The only channels not having a significant correlation were P3P4 and F4. In addition, the baseline values of *width hq* in channel F4 showed significant correlations with conceptional age. *Width hq* channel F3 was the only measure to show any significant differences in the feature values between the groups with different background diagnoses, out of all the calculated features in any frequency bin and channel.

4.4 Correlations between ASI, wPLI and cPSD

In this thesis the correlations between ASI, wPLI and cPSD were also examined to study if there is dependencies between them. These features were chosen as they are all measures that are calculated between pairs of channels. Correlations between the postdrug values of the features are presented in Figure 26, while Figure 27 shows the correlations between the changes in the values after the patients had received dexmedetomidine.

In the figures, the color of each cell represents the Spearman's rank correlation coefficient between two variables, rows and columns. Positive correlations are shown in red, while negative correlations are in blue. If the correlation between the two variables was either insignificant, p-value > 0.05, or the correlation was not strong enough, absolute value of the efficient < 0.2, the correlation is shown in white.

As can be seen in Figure 26 the postdrug values of ASI and cPSD show positive correlations between them, especially the ASI of F4–P4 and the values of cPSD in the frequency bins of 3–8 Hz and 8–15 Hz. However, there seems to be neither positive or negative correlation between ASI and wPLI in any frequency bin. Almost all of the strong correlations between cPSD and wPLI are negative, although there are only a few. The variables of cPSD have the strongest correlations with each other compared to the variables of ASI or wPLI.

With the delta values of ASI, cPSD and wPLI, there seems to be less strong correlations when compared to the strong correlations between the postdrug values. However, between wPLI and cPSD, there can be seen both a few negative correlations as well as a few positive ones.

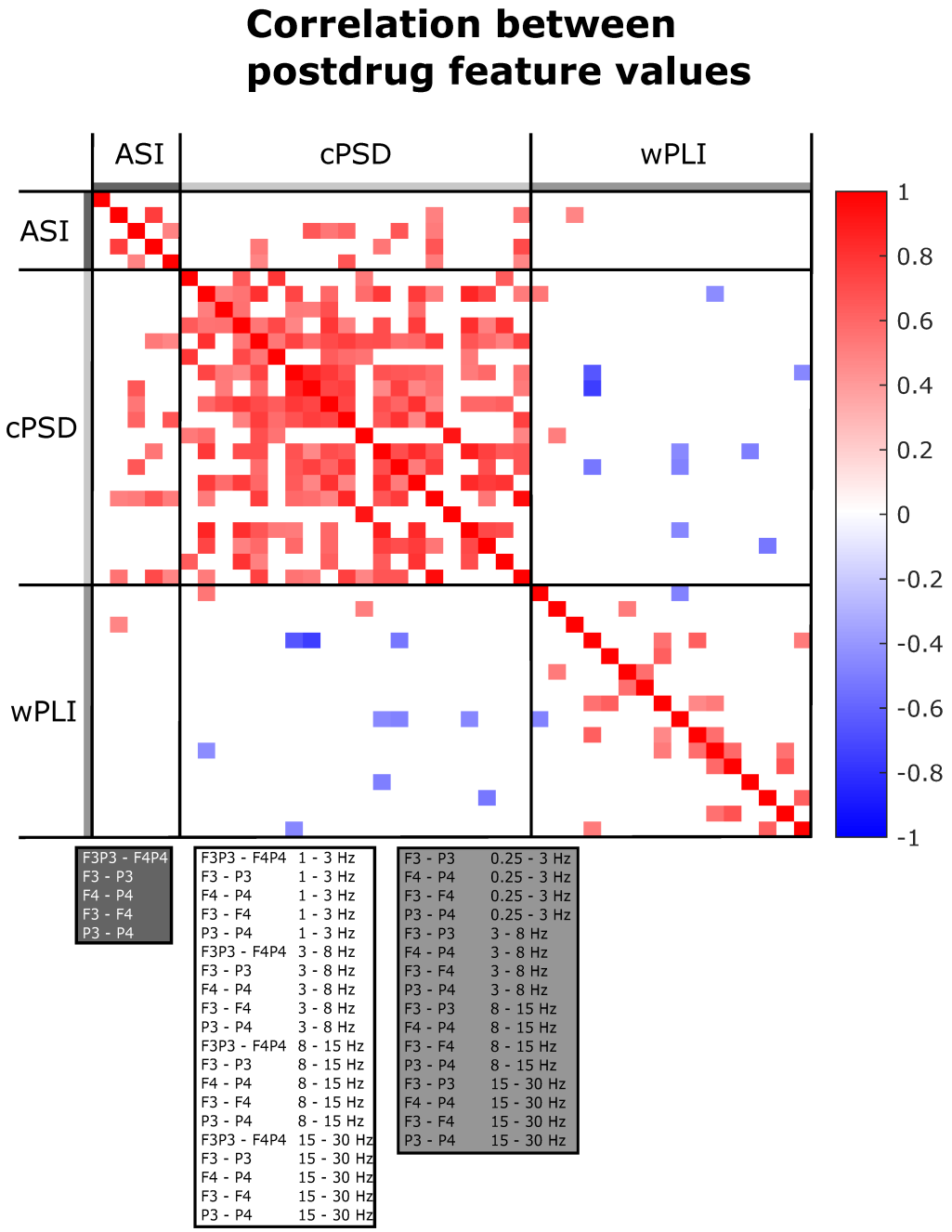

Figure 26: Correlations between the postdrug values of ASI, cPSD and wPLI. Negative correlations are illustrated in shades of blue, while positive correlations are shown in red. White square means that no significant or strong enough correlation between the measures was found.

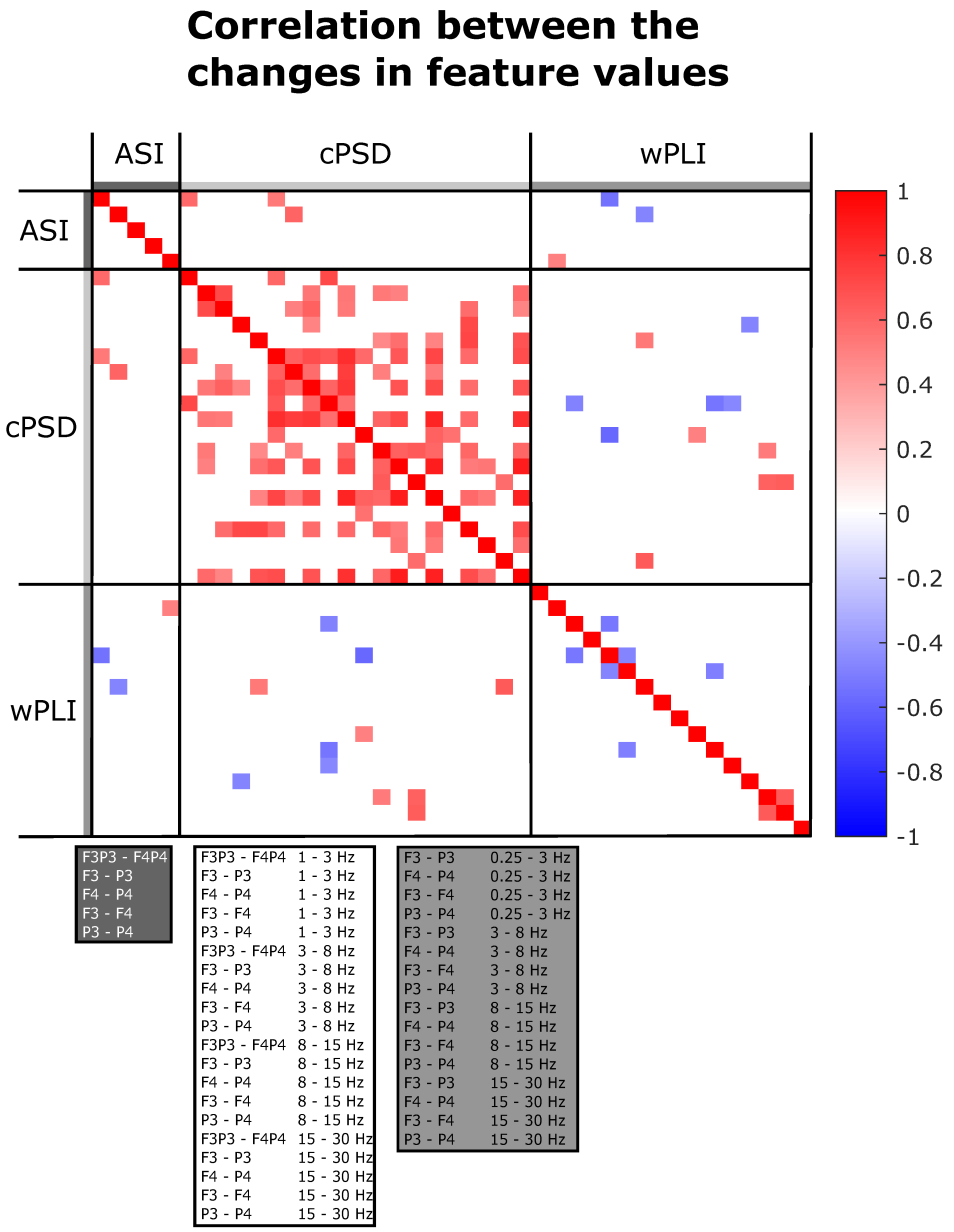

Figure 27: Correlations between the changes in ASI, cPSD and wPLI, after the patients received the drug. Negative correlations are illustrated in shades of blue, while positive correlations are shown in red. White square means that no significant or strong enough correlation between the measures was found.

5 Discussion

The studies carried out in this thesis provide evidence that dexmedetomidine does affect the cortical activity of neonates. They also indicate that the effects take place shortly after the dosing of the drug. The results gathered in the studies are discussed below.

5.1 Differences between features and studies

The lack of results found in the time trends clearly would indicate that dexmedetomidine does not at least have any strong effects that would be clearly seen in the EEG, such as completely wipe out synchronies found with in the brain, such as phase-phase synchrony. However, this could also be due to the different background state of the subjects that supposedly was the cause of the arbitrary time trends even before dexmedetomidine.

The most significant results were found in the short-term studies, as there were multiple strong correlations between the baseline and the change of feature value after the drug. These correlations indicate that dexmedetomidine does affect the cortical activity of the subjects. Although there were a few strong correlations between the post- and predrug values aswell, they are negligible as no post hoc correction was performed.

Most of the significant correlations in short-term studies were found with features that measure synchrony between two regions in the brain: ASI and wPLI. Interestingly, they were all negative, meaning that the greater the baseline value of a feature, the greater the decrease or smaller the increase in the value after the patients received the drug. However, when comparing whether feature value in the pre- or postdrug epoch was greater, no clear consensus was found. Moreover, the effect on synchrony did not seem to be dependant on the region of the brain, as significant correlations were found within all channel pairs of wPLI.

As the correlation between ASI and wPLI was also examined and found not to exist. It can be stated that the significant results of either ASI or wPLI are not dependant on the other. Interestingly none of the ASI, wPLI and cPSD seemed to correlate with each other to a meaningful amount. Also, the different montages within the features seemed to correlate more with the postdrug values than delta values.

As presented in the results, only the MFDFA *peak hq* values expressed correlation with the studied clinical factors in any meaningful amount. However, the feature did not show any correlations with dexmedetomidine. The lack of any correlations in short-term studies could be due to the effect of conceptional age that conceals the effects of dexmedetomidine. Especially as the other variables of MFDFA showed correlations in short-term studies to an extent, especially the *width hq* and *height Dq*. Moreover, neither of these variables expressed correlations with the clinical factors.

Previously dexmedetomidine has been reported to induce brain activity resembling stage II sleep [28, 65]. Mason et al. [65] also found out that dexmedetomidine sedation resulted in increased activity in theta, alpha and beta frequency bands. However, as PSD had only a few significant correlations in the frequencies from 8 to 15 Hz, the sleep like induced sedation of dexmedetomidine cannot be confirmed with our findings. This could be due to the neonates being critically ill and heavily medicated, and thus it is questionable if they would express any sleep stages at all even one induced by medication.

5.2 Technical limitations and strengths

The presence of artifacts proved to be the most challenging technical limitation for our study, as is often the case with EEG studies. For some studies, choosing manually artifact free epochs is suitable, however, for us it was not possible as we had to take into account either the time until or from the moment the subjects received the drug. This was necessary for the data from different subjects to be comparable in both for the time trends as well as the short-term effects.

Another challenge with the study was the different clinical backgrounds between the subjects. As all of the newborns were critically ill, obtaining a homogeneous study group with similar clinical background, i.e. diagnoses and medication, was not possible. And thus, the differing clinical backgrounds could affect the cortical activity of the subjects and the results obtained in this study. Furthermore, as we hypothesized fentanyl could have affected the lack of results found even though most of the features did not express correlation with the patients receiving fentanyl. However, as only the exact time for receiving dexmedetomidine was known and not when the neonates received fentanyl, it could be possible that the some of the subjects received it hours after dexmedetomidine. Thus, the groups of subjects used for studying the effects of fentanyl on the baseline value might have been inaccurate, as we only examined the preceding 12 minutes of dexmedetomidine dosing. On the other hand, Chrysostomou et al. also studied sedation induced by dexmedetomidine and found out that fentanyl does not affect the sedation. [66] Their study subjects included neonates, although did not consist of them exclusively.

One additional limitation caused by the differences between the subjects could be because of the huge variability in conceptional ages of the subjects. The difference in conceptional age between the youngest and the oldest neonate was almost 16 weeks, which is a very long time in the early development of the neonatal brain. Thus the different developmental state of the brain could result in different expressions of the medication.

The most significant technical strength in this study was the chosen feature set. The chosen features measure the cortical activity extensively and versatilely. In addition, the stability of the features used in this study, with the exception of aEEG and rEEG, was studied previously by Julia Jaatela [7]. In her thesis, Jaatela showed that the values of these features do not vary significantly between different epochs and epoch lengths meaning that they are stable over time.

Another strength in the studies conducted, was taking into account various different factors that could affect either the baseline value of the subject, or alter the effect of dexmedetomidine.

5.3 Future prospects

As the effects of dexmedetomidine were left somewhat unclear, other than the fact that they are found shortly after the patients received the drug and affected the synchrony in the brain, more research on the matter needs to be conducted. In addition, repeating the short-term studies with differing time passed since the subjects received dexmedetomidine could be of interest. For example studying epochs from 10 to 20 and from 20 to 30 minutes after the dosing and comparing them to the baseline could provide some new information.

One of the implications provided by the results presented in this thesis is that hour-long recordings of EEG are not necessary for future studies of dexmedetomidine. In addition, the results suggest that dexmedetomidine could affect mainly the synchrony of the brain and thus focusing on features that measure correlations between two regions of the brain could be of interest.

For future studies, focusing on the measurement setup in order to prevent unnecessary artifacts would be a major improvement. This is challenging, however, as the subjects are neonates and controlling them, for example their movements, while doing the measurements is difficult. It could also be argued that a larger sample size than 21 subjects would provide more reliable results.

6 Conclusions

The goal of this thesis was to study whether dexmedetomidine would affect the cortical activity of neonates or not. The effects were studied on different time scales and various different factors that could affect the results were analyzed as presented in the beginning of this thesis. The computational features used in these studies were statistically analyzed for consistent differences between the distributions of pre and postdrug values.

No conclusions on the hour-long lasting effects of dexmedetomidine were able to be deducted based on the time trends and thus dexmedetomidine does not seem to have effects that would last that long. The lack of these kind of results were also speculated to be a result of the critical illness and the different background states of the neonates due to varying medical conditions.

However, in the short-term studies, dexmedetomidine was clearly shown to have an effect on the synchrony within the brain as both ASI and wPLI had significant results. The correlation between these features was also studied and they were shown not to be dependant on each other. Due to the scarce nature of the results and the effects being expressed on different channels and frequencies, no conclusions were able to be made on either the location or the frequencies that dexmedetomidine would specifically affect.

In the last study of different clinical factors effect on the baseline values of the neonates, it was shown that they did not have an effect. Thus the results presented in this thesis can be considered reliable and truthful.

This thesis can be used as preparatory groundwork for following studies as it was shown that hour-long recordings of EEG do not seem to be needed for examining the effects of dexmedetomidine. However, further research is required to confirm these findings.

References

[1] K. P. Mason, S. E. Zgleszewski, R. Prescilla, P. J. Fontaine, and D. Zurakowski, "Hemodynamic effects of dexmedetomidine sedation for ct imaging studies," *Pediatric Anesthesia*, vol. 18, no. 5, pp. 393–402, 2008.

[2] K. P. Mason, S. E. Zgleszewski, J. L. Dearden, R. S. Dumont, M. A. Pirich, C. D. Stark, P. D'angelo, S. MacPherson, P. J. Fontaine, L. Connor *et al.*, "Dexmedetomidine for pediatric sedation for computed tomography imaging studies," 2006.

[3] Z. Ozkose, F. S. Demir, K. Pampal, and S. Yardim, "Hemodynamic and anesthetic advantages of dexmedetomidine, an α2-agonist, for surgery in prone position," *The Tohoku journal of experimental medicine*, vol. 210, no. 2, pp. 153–160, 2006.

[4] A. T. Gerlach, C. V. Murphy, and J. F. Dasta, "An updated focused review of dexmedetomidine in adults," *Annals of Pharmacotherapy*, vol. 43, no. 12, pp. 2064–2074, 2009.

[5] J. Wong, G. M. Steil, M. Curtis, A. Papas, D. Zurakowski, and K. P. Mason, "Cardiovascular effects of dexmedetomidine sedation in children," *Anesthesia & Analgesia*, vol. 114, no. 1, pp. 193–199, 2012.

[6] R. C. Prielipp, M. H. Wall, J. R. Tobin, L. Groban, M. A. Cannon, F. H. Fahey, H. D. Gage, D. A. Stump, R. L. James, J. Bennett *et al.*, "Dexmedetomidine-induced sedation in volunteers decreases regional and global cerebral blood flow," *Anesthesia & Analgesia*, vol. 95, no. 4, pp. 1052–1059, 2002.

[7] J. Jaatela, "Computational features of neonatal eeg monitoring after asphyxia," 2017.

[8] G. J. Tortora and B. H. Derrickson, *Principles of anatomy and physiology*. John Wiley & Sons, 2008.

[9] L. Hellstrom-Westas and I. Rosen, "Electroencephalography and amplitude-integrated eeg," *The Newborn Brain: Neuroscience and Clinical Applications. Cambridge University Press: Cambridge, UK*, pp. 211–228, 2010.

[10] E. Niedermeyer *et al.*, "The normal eeg of the waking adult," *Electroencephalography: Basic principles, clinical applications, and related fields*, vol. 167, pp. 155–164, 2005.

[11] H. H. Jasper, "The ten-twenty electrode system of the international federation," *Electroencephalogr. Clin. Neurophysiol.*, vol. 10, pp. 370–375, 1958.

[12] V. L. Towle, J. Bolaños, D. Suarez, K. Tan, R. Grzeszczuk, D. N. Levin, R. Cakmur, S. A. Frank, and J.-P. Spire, "The spatial location of eeg electrodes: locating the best-fitting sphere relative to cortical anatomy," *Electroencephalography and clinical neurophysiology*, vol. 86, no. 1, pp. 1–6, 1993.

[13] B. Burle, L. Spieser, C. Roger, L. Casini, T. Hasbroucq, and F. Vidal, "Spatial and temporal resolutions of eeg: Is it really black and white? a scalp current density view," *International Journal of Psychophysiology*, vol. 97, no. 3, pp. 210–220, 2015.

[14] S. B. Rutkove, "Introduction to volume conduction," in *The clinical neurophysiology primer*. Springer, 2007, pp. 43–53.

[15] D. M. White and C. A. Van Cott, "Eeg artifacts in the intensive care unit setting," *American journal of electroneurodiagnostic technology*, vol. 50, no. 1, pp. 8–25, 2010.

[16] P. Anderer, S. Roberts, A. Schlögl, G. Gruber, G. Klösch, W. Herrmann, P. Rappelsberger, O. Filz, M. J. Barbanoj, G. Dorffner *et al.*, "Artifact processing in computerized analysis of sleep eeg–a review," *Neuropsychobiology*, vol. 40, no. 3, pp. 150–157, 1999.

[17] E. L. Reilly, "Eeg recordings and operation of the apparatus," *Electroencephalography. Basic principles, clinical applications and related fields*, pp. 139–159, 2005.

[18] A. Kamp, G. Pfurtscheller, G. Edlinger, and F. L. da Silva, "Technological basis of eeg recording," *Electroencephalography. Basic principles, clinical applications and related fields*, pp. 127–138, 2005.

[19] J. Stiles and T. L. Jernigan, "The basics of brain development," *Neuropsychology review*, vol. 20, no. 4, pp. 327–348, 2010.

[20] D. H. Sanes, T. A. Reh, and W. A. Harris, *Development of the nervous system*. Elsevier, 2005.

[21] E. Niedermeyer *et al.*, "Maturation of the eeg: development of waking and sleep patterns," *Electroencephalography: Basic principles, clinical applications, and related fields*, vol. 167, pp. 209–234, 2005.

[22] K. Malk, M. Metsäranta, and S. Vanhatalo, "Drug effects on endogenous brain activity in preterm babies," *Brain and Development*, vol. 36, no. 2, pp. 116–123, 2014.

[23] I. Kostović and N. Jovanov-Milošević, "The development of cerebral connections during the first 20–45 weeks' gestation," in *Seminars in Fetal and Neonatal Medicine*, vol. 11, no. 6. Elsevier, 2006, pp. 415–422.

[24] S. Vanhatalo and K. Kaila, "Emergence of spontaneous and evoked electroencephalographic activity in the human brain."

[25] M. J. Aminoff, *Aminoff's Electrodiagnosis in Clinical Neurology E-Book*. Elsevier Health Sciences, 2012.

[26] E. A. Martin, T. A. McFerran *et al.*, *A dictionary of nursing*. Oxford University Press, 2014.

[27] S. Shankaran, A. R. Laptook, R. A. Ehrenkranz, J. E. Tyson, S. A. McDonald, E. F. Donovan, A. A. Fanaroff, W. K. Poole, L. L. Wright, R. D. Higgins *et al.*, "Whole-body hypothermia for neonates with hypoxic–ischemic encephalopathy," *New England Journal of Medicine*, vol. 353, no. 15, pp. 1574–1584, 2005.

[28] K. P. Mason and J. Lerman, "Dexmedetomidine in children: current knowledge and future applications," *Anesthesia & Analgesia*, vol. 113, no. 5, pp. 1129–1142, 2011.

[29] C. Chrysostomou, S. R. Schulman, M. H. Castellanos, B. E. Cofer, S. Mitra, M. G. da Rocha, W. A. Wisemandle, and L. Gramlich, "A phase ii/iii, multicenter, safety, efficacy, and pharmacokinetic study of dexmedetomidine in preterm and term neonates," *The Journal of pediatrics*, vol. 164, no. 2, pp. 276–282, 2014.

[30] A. W. Loepke and S. G. Soriano, "An assessment of the effects of general anesthetics on developing brain structure and neurocognitive function," *Anesthesia & Analgesia*, vol. 106, no. 6, pp. 1681–1707, 2008.

[31] A. J. Davidson, "Anesthesia and neurotoxicity to the developing brain: the clinical relevance," *Pediatric Anesthesia*, vol. 21, no. 7, pp. 716–721, 2011.

[32] G. Stratmann, "Neurotoxicity of anesthetic drugs in the developing brain," *Anesthesia & Analgesia*, vol. 113, no. 5, pp. 1170–1179, 2011.

[33] A. Wauquier, "Eeg and neuropharmacology," *Electroencephalography: Basic Principles, Clinical Applications and Related Fields-Fifth Edition", Williams & Wilkins, Baltimore, MD*, 2005.

[34] F. da Silva, "Eeg analysis: Theory and practice," *Electroencephalography: Basic Principles, Clinical Applications and Related Fields-Fifth Edition", Williams & Wilkins, Baltimore, MD*, pp. 1199–1231, 2005.

[35] G. Boylan, L. Burgoyne, C. Moore, B. O'Flaherty, and J. Rennie, "An international survey of eeg use in the neonatal intensive care unit," *Acta Paediatrica*, vol. 99, no. 8, pp. 1150–1155, 2010.

[36] L. Hellström-Westas and I. Rosén, "Continuous brain-function monitoring: state of the art in clinical practice," in *Seminars in Fetal and Neonatal Medicine*, vol. 11, no. 6. Elsevier, 2006, pp. 503–511.

[37] G. Bauer and R. Bauer, "Eeg, drug effects and central nervous system poisonging," *Electroencephalography: Basic Principles, Clinical Applications and Related Fields-Fifth Edition", Williams & Wilkins, Baltimore, MD*, pp. 701–723, 2005.

[38] O. Räsänen, M. Metsäranta, and S. Vanhatalo, "Development of a novel robust measure for interhemispheric synchrony in the neonatal eeg: activation synchrony index (asi)," *Neuroimage*, vol. 69, pp. 256–266, 2013.

[39] N. Koolen, A. Dereymaeker, O. Räsänen, K. Jansen, J. Vervisch, V. Matic, G. Naulaers, M. De Vos, S. Van Huffel, and S. Vanhatalo, "Early development of synchrony in cortical activations in the human," *Neuroscience*, vol. 322, pp. 298–307, 2016.

[40] A. Tokariev, K. Palmu, A. Lano, M. Metsäranta, and S. Vanhatalo, "Phase synchrony in the early preterm eeg: development of methods for estimating synchrony in both oscillations and events," *Neuroimage*, vol. 60, no. 2, pp. 1562–1573, 2012.

[41] A. M. Bastos and J.-M. Schoffelen, "A tutorial review of functional connectivity analysis methods and their interpretational pitfalls," *Frontiers in systems neuroscience*, vol. 9, 2015.

[42] J.-P. Lachaux, E. Rodriguez, J. Martinerie, F. J. Varela *et al.*, "Measuring phase synchrony in brain signals," *Human brain mapping*, vol. 8, no. 4, pp. 194–208, 1999.

[43] C. J. Stam, G. Nolte, and A. Daffertshofer, "Phase lag index: assessment of functional connectivity from multi channel eeg and meg with diminished bias from common sources," *Human brain mapping*, vol. 28, no. 11, pp. 1178–1193, 2007.

[44] M. Vinck, R. Oostenveld, M. Van Wingerden, F. Battaglia, and C. M. Pennartz, "An improved index of phase-synchronization for electrophysiological data in the presence of volume-conduction, noise and sample-size bias," *Neuroimage*, vol. 55, no. 4, pp. 1548–1565, 2011.

[45] S. Vanhatalo, J. M. Palva, S. Andersson, C. Rivera, J. Voipio, and K. Kaila, "Slow endogenous activity transients and developmental expression of k+–cl- cotransporter 2 in the immature human cortex," *European Journal of Neuroscience*, vol. 22, no. 11, pp. 2799–2804, 2005.

[46] A. B. Tort, R. Komorowski, H. Eichenbaum, and N. Kopell, "Measuring phase-amplitude coupling between neuronal oscillations of different frequencies," *Journal of neurophysiology*, vol. 104, no. 2, pp. 1195–1210, 2010.

[47] A. Tokariev, M. Videman, J. M. Palva, and S. Vanhatalo, "Functional brain connectivity develops rapidly around term age and changes between vigilance states in the human newborn," *Cerebral Cortex*, vol. 26, no. 12, pp. 4540–4550, 2016.

[48] S. Monto, S. Palva, J. Voipio, and J. M. Palva, "Very slow eeg fluctuations predict the dynamics of stimulus detection and oscillation amplitudes in humans," *Journal of Neuroscience*, vol. 28, no. 33, pp. 8268–8272, 2008.

[49] S. Palva and J. M. Palva, "Discovering oscillatory interaction networks with m/eeg: challenges and breakthroughs," *Trends in cognitive sciences*, vol. 16, no. 4, pp. 219–230, 2012.

[50] M. Thordstein, A. Flisberg, N. Löfgren, R. Bågenholm, K. Lindecrantz, B. Wallin, and I. Kjellmer, "Spectral analysis of burst periods in eeg from healthy and post-asphyctic full-term neonates," *Clinical neurophysiology*, vol. 115, no. 11, pp. 2461–2466, 2004.

[51] P. Welch, "The use of fast fourier transform for the estimation of power spectra: a method based on time averaging over short, modified periodograms," *IEEE Transactions on audio and electroacoustics*, vol. 15, no. 2, pp. 70–73, 1967.

[52] L. Hellström-Westas, I. Rosén, L. De Vries, and G. Greisen, "Amplitude-integrated eeg classification and interpretation in preterm and term infants," *NeoReviews*, vol. 7, no. 2, pp. e76–e87, 2006.

[53] N. al Naqeeb, A. D. Edwards, F. M. Cowan, and D. Azzopardi, "Assessment of neonatal encephalopathy by amplitude-integrated electroencephalography," *Pediatrics*, vol. 103, no. 6, pp. 1263–1271, 1999.

[54] D. O'Reilly, M. A. Navakatikyan, M. Filip, D. Greene, and L. J. Van Marter, "Peak-to-peak amplitude in neonatal brain monitoring of premature infants," *Clinical Neurophysiology*, vol. 123, no. 11, pp. 2139–2153, 2012.

[55] E. A. Ihlen, "Introduction to multifractal detrended fluctuation analysis in matlab," *Frontiers in physiology*, vol. 3, 2012.

[56] G. Wang, H. Huang, H. Xie, Z. Wang, and X. Hu, "Multifractal analysis of ventricular fibrillation and ventricular tachycardia," *Medical engineering & physics*, vol. 29, no. 3, pp. 375–379, 2007.

[57] Y. Zheng, J. Gao, J. C. Sanchez, J. C. Principe, and M. S. Okun, "Multiplicative multifractal modeling and discrimination of human neuronal activity," *Physics Letters A*, vol. 344, no. 2, pp. 253–264, 2005.

[58] J. W. Kantelhardt, S. A. Zschiegner, E. Koscielny-Bunde, S. Havlin, A. Bunde, and H. E. Stanley, "Multifractal detrended fluctuation analysis of nonstationary time series," *Physica A: Statistical Mechanics and its Applications*, vol. 316, no. 1, pp. 87–114, 2002.

[59] V. Matic, P. J. Cherian, N. Koolen, A. H. Ansari, G. Naulaers, P. Govaert, S. Van Huffel, M. De Vos, and S. Vanhatalo, "Objective differentiation of neonatal eeg background grades using detrended fluctuation analysis," *Frontiers in human neuroscience*, vol. 9, 2015.

[60] T. Zorick and M. A. Mandelkern, "Multifractal detrended fluctuation analysis of human eeg: preliminary investigation and comparison with the wavelet transform modulus maxima technique," *PloS one*, vol. 8, no. 7, p. e68360, 2013.

[61] F. Wilcoxon, "Individual comparisons by ranking methods," *Biometrics bulletin*, vol. 1, no. 6, pp. 80–83, 1945.

[62] J. D. Gibbons and S. Chakraborti, *Nonparametric Statistical Inference*. CRC Press, 2003, vol. 168.

[63] Y. Chan and R. P. Walmsley, "Learning and understanding the kruskal-wallis one-way analysis-of-variance-by-ranks test for differences among three or more independent groups," *Physical therapy*, vol. 77, no. 12, pp. 1755–1761, 1997.

[64] J. H. Zar, "Significance testing of the spearman rank correlation coefficient," *Journal of the American Statistical Association*, vol. 67, no. 339, pp. 578–580, 1972.

[65] K. P. Mason, E. O'MAHONY, D. Zurakowski, and M. H. Libenson, "Effects of dexmedetomidine sedation on the eeg in children," *Pediatric Anesthesia*, vol. 19, no. 12, pp. 1175–1183, 2009.

[66] C. Chrysostomou, J. S. De Toledo, T. Avolio, M. V. Motoa, D. Berry, V. O. Morell, R. Orr, and R. Munoz, "Dexmedetomidine use in a pediatric cardiac intensive care unit: can we use it in infants after cardiac surgery?" *Pediatric Critical Care Medicine*, vol. 10, no. 6, pp. 654–660, 2009.

A Appendix A

In this appendix, the results of all of the features are listed in their own tables and the feature in question is specified in the label. Results for different frequency and channel combinations are presented in their own rows. The second column the p-value for Wilcoxon signed-rank test between the postdrug and predrug values are listed. In the next column (DX/BL ↑), the epoch that had the greater feature value is stated, BL = baseline and DX = postdrug. The correlation coefficient (Δ/BL (rho)) and p-value (Δ/BL (p-value)) for Spearman's rank correlation between the delta values and baseline values are given in the following two columns. In the Fentanyl-column the p-values for Wilcoxon's rank sum tests are listed. While the CA labeled columns consist of the correlation coefficient (rho) and p-value for Spearman's correlation tests between the conceptional age and baseline values. In the last column in the tables are listed the p-values of Kruskal-Wallis test for different background diagnoses. In the tables, p-values of less than 0.05 are highlighted in red while values of $0.10 >$ p-value > 0.05 are highlighted in green.

Table A1: ASI

Channel:	DX/BL (p-value)	DX/BL ↑	Δ/BL (rho)	Δ/BL (p-value)	Fentanyl (p-value)	CA (rho)	CA (p-value)	Diagnosis (p-value)
F3P3 — F4P4	0.569	BL	-0.753	0.001	0.023	0.397	0.128	0.500
F3 — P3	0.936	BL	-0.214	0.377	0.837	-0.068	0.783	0.324
F4 — P4	0.064	DX	-0.548	0.020	0.173	0.030	0.906	0.993
F3 — F4	0.446	BL	-0.496	0.038	0.930	0.099	0.696	0.212
P3 — P4	0.126	DX	-0.160	0.512	0.206	0.262	0.279	0.407

Table A2: wPLI

Frequency band:	Channel:	DX/BL (p-value)	DX/BL ↑	Δ/BL (rho)	Δ/BL (p-value)	Fentanyl (p-value)	CA (rho)	CA (p-value)	Diagnosis (p-value)
0.25 — 3 Hz	F3 — P3	0.778	DX	-0.593	0.005	0.152	0.204	0.403	0.698
0.25 — 3 Hz	F4 — P4	0.948	BL	-0.408	0.072	0.600	0.255	0.293	0.318
0.25 — 3 Hz	F3 — F4	0.823	DX	-0.719	0.000	0.298	0.577	0.008	0.939
0.25 — 3 Hz	P3 — P4	0.687	BL	-0.444	0.111	0.965	-0.170	0.499	0.763
3 — 8 Hz	F3— P3	0.263	BL	-0.839	0.000	0.049	-0.350	0.130	0.332
3 — 8 Hz	F4 — P4	0.494	DX	-0.412	0.195	0.840	-0.004	0.986	0.740
3 — 8 Hz	F3 — F4	0.911	DX	-0.462	0.011	0.418	0.114	0.631	0.162
3 — 8 Hz	P3 — P4	0.573	DX	-0.753	0.000	0.968	-0.031	0.901	0.734
8 — 15 Hz	F3 — P3	0.411	BL	-0.835	0.054	0.671	-0.259	0.270	0.481
8 — 15 Hz	F4 — P4	0.126	BL	-0.733	0.001	0.442	0.186	0.445	0.670
8 — 15 Hz	F3 — F4	0.044	BL	-0.580	0.000	0.114	0.004	0.987	0.784
8 — 15 Hz	P3 — P4	0.184	DX	-0.728	0.662	0.717	-0.204	0.403	0.231
15 — 30 Hz	F3 — P3	0.243	DX	-0.826	0.743	0.536	-0.083	0.734	0.268
15 — 30 Hz	F4— P4	0.420	BL	-0.709	0.013	0.965	0.165	0.512	0.109
15 — 30 Hz	F3 — F4	0.845	DX	-0.763	0.056	0.536	-0.066	0.794	0.337
15 — 30 Hz	P3 — P4	0.936	DX	-0.537	0.049	0.310	-0.143	0.559	0.690

Table A3: NC

Frequency band:	Channel:	DX/BL (p-value)	DX/BL ↑	Δ/BL (rho)	Δ/BL (p-value)	Fentanyl (p-value)	CA (rho)	CA (p-value)	Diagnosis (p-value)
3 — 8 Hz	F3	0.062	BL	-0.050	0.836	0.375	0.315	0.177	0.275
3 — 8 Hz	F4	0.550	DX	-0.460	0.043	0.728	0.383	0.096	0.620
3 — 8 Hz	P3	0.167	DX	-0.429	0.061	0.908	-0.092	0.700	0.814
3 — 8 Hz	P4	0.084	DX	-0.449	0.055	0.717	-0.262	0.279	0.523
8 — 15 Hz	F3	0.794	DX	-0.302	0.195	0.059	0.443	0.050	0.107
8 — 15 Hz	F4	0.654	BL	-0.746	0.000	0.908	0.246	0.296	0.090
8 — 15 Hz	P3	0.433	DX	-0.295	0.207	0.335	-0.138	0.560	0.447
8 — 15 Hz	P4	0.872	DX	-0.232	0.339	0.778	0.005	0.983	0.959
15 — 30 Hz	F3	0.904	BL	-0.218	0.369	0.773	-0.323	0.177	0.854
15 — 30 Hz	F4	0.546	DX	-0.519	0.024	0.717	0.111	0.652	0.080
15 — 30 Hz	P3	0.778	BL	-0.228	0.346	0.657	-0.020	0.935	0.681
15 — 30 Hz	P4	0.215	DX	-0.251	0.314	0.904	0.223	0.359	0.574

Table A4: PSD

Frequency band:	Channel:	DX/BL (p-value)	DX/BL ↑	Δ/BL (rho)	Δ/BL (p-value)	Fentanyl (p-value)	CA (rho)	CA (p-value)	Diagnosis (p-value)
1 — 3 Hz	F3P3	0.627	BL	-0.310	0.183	0.787	0.123	0.606	0.344
1 — 3 Hz	F4P4	0.809	BL	-0.186	0.444	0.442	0.024	0.923	0.486
1 — 3 Hz	F3F4	0.218	BL	-0.632	0.003	0.232	0.201	0.396	0.164
1 — 3 Hz	P3P4	0.629	BL	-0.442	0.060	0.717	-0.087	0.723	0.562
1 — 3 Hz	F3	0.411	BL	-0.296	0.204	0.671	0.090	0.705	0.507
1 — 3 Hz	F4	0.455	BL	-0.392	0.088	0.203	0.083	0.729	0.390
1 — 3 Hz	P3	1.000	DX	-0.292	0.211	0.969	-0.012	0.960	0.995
1 — 3 Hz	P4	0.872	DX	-0.356	0.135	0.778	-0.106	0.665	0.681
3 — 8 Hz	F3P3	0.970	DX	-0.155	0.513	0.908	0.035	0.885	0.949
3 — 8 Hz	F4P4	0.717	BL	-0.039	0.877	1.000	-0.075	0.761	0.870
3 — 8 Hz	F3F4	0.601	BL	-0.030	0.901	0.563	0.152	0.522	0.731
3 — 8 Hz	P3P4	0.546	BL	-0.021	0.934	0.840	-0.208	0.393	0.892
3 — 8 Hz	F3	0.911	BL	-0.335	0.148	0.787	0.087	0.717	0.588
3 — 8 Hz	F4	0.654	BL	-0.286	0.221	0.512	0.132	0.578	0.731
3 — 8 Hz	P3	0.737	DX	-0.090	0.705	0.847	-0.029	0.905	0.994
3 — 8 Hz	P4	1.000	BL	-0.344	0.150	0.717	-0.220	0.365	0.930
8 — 15 Hz	F3P3	0.263	BL	-0.171	0.468	1.000	-0.034	0.887	0.962
8 — 15 Hz	F4P4	0.748	BL	-0.167	0.494	0.778	-0.043	0.861	0.876
8 — 15 Hz	F3F4	0.156	BL	-0.528	0.018	0.787	-0.023	0.925	0.584
8 — 15 Hz	P3P4	0.421	BL	0.074	0.765	0.968	-0.295	0.220	0.931
8 — 15 Hz	F3	0.296	DX	-0.493	0.029	0.847	-0.045	0.850	0.840
8 — 15 Hz	F4	0.313	BL	-0.678	0.001	0.512	0.061	0.799	0.653
8 — 15 Hz	P3	0.881	BL	-0.135	0.568	0.728	-0.203	0.390	0.964
8 — 15 Hz	P4	0.904	BL	-0.247	0.306	0.717	-0.296	0.219	0.942
15 — 30 Hz	F3P3	0.573	DX	-0.209	0.389	0.650	0.107	0.663	0.440
15 — 30 Hz	F4P4	0.845	BL	-0.447	0.065	0.460	-0.053	0.836	0.901
15 — 30 Hz	F3F4	0.913	BL	-0.185	0.462	1.000	-0.027	0.916	0.182
15 — 30 Hz	P3P4	0.968	BL	-0.211	0.385	0.717	-0.289	0.230	0.986
15 — 30 Hz	F3	0.936	BL	-0.158	0.517	1.000	0.084	0.732	0.417
15 — 30 Hz	F4	0.573	BL	-0.309	0.198	0.310	0.118	0.631	0.443
15 — 30 Hz	P3	0.970	BL	-0.132	0.577	0.728	-0.080	0.738	0.933
15 — 30 Hz	P4	0.573	DX	-0.335	0.161	0.904	-0.274	0.256	0.940

Table A5: cPSD

Frequency band:	Channel:	DX/BL (p-value)	DX/BL ↑	Δ/BL (rho)	Δ/BL (p-value)	Fentanyl (p-value)	CA (rho)	CA (p-value)	Diagnosis (p-value)
1 — 3 Hz	F3P3 — F4P4	0.948	DX	-0.393	0.107	0.829	-0.120	0.636	0.529
1 — 3 Hz	F3 — P3	0.881	BL	-0.445	0.051	0.375	0.040	0.867	0.493
1 — 3 Hz	F4 — P4	0.049	BL	-0.367	0.123	0.968	-0.039	0.875	0.628
1 — 3 Hz	F3 — F4	0.313	DX	0.032	0.896	0.969	-0.093	0.698	0.448
1 — 3 Hz	P3 — P4	0.841	DX	-0.354	0.137	0.717	0.261	0.281	0.482
3 — 8 Hz	F3P3 — F4P4	0.647	BL	-0.333	0.176	0.829	-0.134	0.595	0.862
3 — 8 Hz	F3 — P3	1.000	BL	-0.153	0.517	0.616	0.284	0.224	0.802
3 — 8 Hz	F4 — P4	0.687	DX	-0.193	0.427	0.968	0.083	0.737	0.945
3 — 8 Hz	F3 — F4	0.279	DX	-0.729	0.000	0.908	0.027	0.910	0.655
3 — 8 Hz	P3 — P4	0.936	BL	-0.195	0.423	0.657	-0.130	0.596	0.906
8 — 15 Hz	F3P3 — F4P4	0.094	BL	-0.523	0.028	1.000	0.161	0.523	0.512
8 — 15 Hz	F3 — P3	0.765	DX	-0.577	0.009	0.671	0.041	0.865	0.932
8 — 15 Hz	F4 — P4	0.936	BL	-0.282	0.240	0.351	-0.238	0.327	0.955
8 — 15 Hz	F3 — F4	0.455	DX	-0.492	0.029	0.969	0.108	0.649	0.549
8 — 15 Hz	P3 — P4	0.904	DX	-0.230	0.342	0.395	-0.011	0.966	0.799
15 — 30 Hz	F3P3 — F4P4	0.836	BL	0.088	0.746	0.681	-0.175	0.517	0.685
15 — 30 Hz	F3 — P3	0.841	DX	-0.233	0.335	0.482	-0.066	0.789	0.917
15 — 30 Hz	F4 — P4	0.811	BL	-0.253	0.310	0.829	-0.209	0.406	0.318
15 — 30 Hz	F3 — F4	0.420	DX	-0.195	0.436	0.536	-0.118	0.642	0.985
15 — 30 Hz	P3 — P4	0.212	DX	-0.060	0.809	0.545	-0.136	0.579	0.911

Table A6: aEEG mean

Channel:	DX/BL (p-value)	DX/BL ↑	Δ/BL (rho)	Δ/BL (p-value)	Fentanyl (p-value)	CA (rho)	CA (p-value)	Diagnosis (p-value)
F3P3	0.398	DX	-0.368	0.121	0.840	0.196	0.422	0.645
F4P4	0.398	BL	-0.396	0.094	0.310	0.133	0.586	0.536
F3F4	0.852	BL	-0.203	0.389	0.375	0.274	0.243	0.325
P3P4	0.494	BL	-0.349	0.143	0.492	-0.093	0.705	0.891
F3	0.881	BL	-0.438	0.055	0.512	0.184	0.437	0.696
F4	0.911	DX	-0.271	0.247	0.512	0.251	0.285	0.469
P3	0.502	DX	-0.110	0.644	1.000	0.014	0.955	0.961
P4	0.687	DX	-0.419	0.075	0.840	0.013	0.957	0.726

Table A7: aEEG IQR

Channel:	DX/BL (p-value)	DX/BL ↑	Δ/BL (rho)	Δ/BL (p-value)	Fentanyl (p-value)	CA (rho)	CA (p-value)	Diagnosis (p-value)
F3P3	0.227	DX	0.200	0.410	0.968	-0.119	0.626	0.989
F4P4	0.520	DX	0.107	0.662	0.778	-0.169	0.488	0.946
F3F4	0.823	DX	-0.174	0.460	0.512	-0.087	0.714	0.794
P3P4	0.841	BL	0.049	0.843	0.968	-0.295	0.220	0.903
F3	0.575	BL	-0.081	0.733	0.969	-0.162	0.496	0.866
F4	0.033	BL	0.186	0.429	0.908	-0.115	0.629	0.868
P3	0.073	BL	0.143	0.547	0.847	-0.223	0.344	0.951
P4	0.421	BL	-0.204	0.402	0.968	-0.181	0.459	0.753

Table A8: rEEG mean

Channel:	DX/BL (p-value)	DX/BL ↑	Δ/BL (rho)	Δ/BL (p-value)	Fentanyl (p-value)	CA (rho)	CA (p-value)	Diagnosis (p-value)
F3P3	0.748	DX	-0.346	0.147	0.902	0.114	0.642	0.529
F4P4	0.744	DX	-0.300	0.225	0.360	-0.124	0.624	0.502
F3F4	0.777	BL	-0.296	0.232	0.536	0.101	0.690	0.139
P3P4	0.445	BL	-0.414	0.079	0.545	-0.104	0.673	0.456
F3	0.421	BL	-0.612	0.006	0.711	0.192	0.431	0.409
F4	0.658	DX	-0.440	0.061	0.238	0.050	0.839	0.425
P3	0.823	DX	-0.205	0.385	0.969	-0.004	0.987	0.986
P4	0.717	DX	-0.489	0.035	0.840	-0.093	0.705	0.600

Table A9: rEEG IQR

Channel:	DX/BL (p-value)	DX/BL ↑	Δ/BL (rho)	Δ/BL (p-value)	Fentanyl (p-value)	CA (rho)	CA (p-value)	Diagnosis (p-value)
F3P3	0.778	DX	-0.128	0.600	0.773	-0.147	0.547	0.796
F4P4	0.811	BL	-0.245	0.327	0.573	-0.154	0.542	0.589
F3F4	0.777	BL	-0.069	0.786	0.659	-0.239	0.341	0.398
P3P4	0.778	DX	-0.291	0.226	1.000	-0.189	0.439	0.666
F3	0.334	DX	-0.423	0.073	0.902	-0.090	0.716	0.872
F4	0.748	BL	0.023	0.928	0.395	-0.041	0.867	0.515
P3	0.970	BL	0.047	0.846	1.000	-0.194	0.412	0.826
P4	0.445	BL	-0.275	0.253	0.840	-0.162	0.506	0.666

Table A10: rEEG LI

Channel:	DX/BL (p-value)	DX/BL ↑	Δ/BL (rho)	Δ/BL (p-value)	Fentanyl (p-value)	CA (rho)	CA (p-value)	Diagnosis (p-value)
F3P3	0.778	BL	-0.170	0.485	0.536	0.432	0.065	0.340
F4P4	0.711	BL	-0.226	0.366	0.083	0.083	0.744	0.600
F3F4	0.616	DX	-0.067	0.792	0.151	0.465	0.052	0.264
P3P4	0.778	BL	-0.184	0.449	0.310	0.133	0.586	0.248
F3	0.629	DX	-0.447	0.056	0.340	0.528	0.020	0.293
F4	0.968	BL	-0.428	0.069	0.091	0.348	0.145	0.314
P3	0.765	BL	-0.156	0.509	0.908	0.283	0.227	0.436
P4	0.841	DX	-0.349	0.143	0.545	0.056	0.819	0.169

Table A11: MFDFA peak hq

Channel:	DX/BL (p-value)	DX/BL ↑	Δ/BL (rho)	Δ/BL (p-value)	Fentanyl (p-value)	CA (rho)	CA (p-value)	Diagnosis (p-value)
F3P3	0.133	DX	0.443	0.067	1.000	-0.515	0.029	0.320
F4P4	0.177	BL	-0.044	0.869	0.965	-0.558	0.016	0.279
F3F4	0.064	BL	0.191	0.446	0.596	-0.478	0.045	0.133
P3P4	0.619	DX	-0.071	0.787	0.515	-0.386	0.113	0.094
F3	0.778	DX	0.042	0.865	0.650	-0.476	0.040	0.289
F4	0.314	DX	0.346	0.147	0.545	-0.369	0.120	0.470
P3	0.355	BL	0.160	0.512	0.492	-0.460	0.047	0.146
P4	0.071	BL	0.026	0.921	0.600	-0.552	0.014	0.058

Table A12: MFDFA width hq

Channel:	DX/BL (p-value)	DX/BL ↑	Δ/BL (rho)	Δ/BL (p-value)	Fentanyl (p-value)	CA (rho)	CA (p-value)	Diagnosis (p-value)
F3P3	0.811	DX	-0.486	0.043	0.860	-0.129	0.610	0.300
F4P4	0.687	BL	-0.176	0.497	0.696	-0.269	0.281	0.716
F3F4	0.006	DX	-0.397	0.104	0.791	-0.363	0.138	0.139
P3P4	0.981	DX	-0.338	0.184	0.633	-0.362	0.140	0.648
F3	0.314	DX	-0.488	0.036	0.711	-0.366	0.123	0.044
F4	0.227	BL	-0.196	0.418	0.351	-0.481	0.037	0.474
P3	0.658	DX	-0.572	0.012	0.600	-0.127	0.604	0.727
P4	0.711	DX	-0.575	0.014	0.600	-0.276	0.253	0.834

Table A13: MFDFA tail Dq

Channel:	DX/BL (p-value)	DX/BL ↑	Δ/BL (rho)	Δ/BL (p-value)	Fentanyl (p-value)	CA (rho)	CA (p-value)	Diagnosis (p-value)
F3P3	0.184	DX	-0.292	0.239	0.596	-0.007	0.977	0.866
F4P4	0.177	DX	-0.407	0.106	0.315	-0.080	0.754	0.899
F3F4	0.396	DX	-0.383	0.118	0.056	0.320	0.195	0.897
P3P4	0.044	DX	-0.566	0.020	0.460	0.020	0.938	0.468
F3	0.904	BL	-0.565	0.013	0.837	0.171	0.484	0.340
F4	0.077	BL	-0.418	0.077	0.492	0.169	0.490	0.718
P3	0.968	BL	-0.193	0.427	0.272	0.137	0.576	0.302
P4	0.349	DX	-0.203	0.417	0.657	0.023	0.926	0.398

Table A14: MFDFA height Dq

Channel:	DX/BL (p-value)	DX/BL ↑	Δ/BL (rho)	Δ/BL (p-value)	Fentanyl (p-value)	CA (rho)	CA (p-value)	Diagnosis (p-value)
F3P3	0.845	DX	-0.624	0.007	0.536	0.034	0.893	0.934
F4P4	0.246	DX	-0.632	0.008	0.696	-0.003	0.990	0.964
F3F4	0.112	DX	-0.073	0.773	0.069	-0.249	0.319	0.572
P3P4	0.102	BL	-0.728	0.001	0.829	-0.083	0.744	0.813
F3	0.494	BL	-0.556	0.015	0.432	0.147	0.547	0.097
F4	0.398	DX	-0.335	0.161	1.000	-0.291	0.226	0.999
P3	0.184	DX	-0.640	0.004	0.020	0.039	0.875	0.838
P4	0.879	DX	-0.668	0.003	0.840	-0.002	0.994	0.993